Optimization of fibre positions in arbitrary tumour geometries for interstitial photodynamic therapy

Andreas Eriksson
Jonas Hjelm

Master's Thesis

Lund Reports on Atomic Physics, LRAP-332
Lund, October 2004

Abstract

Interstitial photodynamic therapy (IPDT) is a laser based method for the treatment of malignant tumours, where the therapeutic light is delivered by means of optical fibres inserted into the tumour mass. This Master's thesis describes the development of an algorithm for optimal fibre placement in IPDT. The algorithm is a type of stochastic iterative method that manages to optimize the positions of an arbitrary number of treatment fibres in an arbitrarily shaped tumour within a 2 minute calculation time. The algorithm has been tested on several tumour geometries of different sizes and shapes. Sensitive tissues, in the vicinity of the tumour, are also taken into consideration during the optimization process. The performance of the algorithm has been compared both to manual positioning and a genetic algorithm also developed during this project. The tests have shown that the solutions proposed by the algorithm are optimal or close to optimal for the used objective function.

Contents

1 Introduction

Cancer is a fatal disease that plagues a large and increasing part of the population. Much effort is therefore spent nowadays on trying to improve cancer treatment. One new promising treatment method is interstitial photodynamic therapy, IPDT. The principle of IPDT is to deliver laser light into the tumour mass through optical fibres. This method has been developed and evaluated at the Atomic Physics Department at the Lund Institute of Technology and is now further developed by the spin-off company SpectraCure AB. The main advantages of IPDT compared to other treatment methods are that there are few side-effects due to the use of non-ionizing radiation and the high selectivity for tumour tissue.

The purpose of this Master's project is to develop an algorithm that calculates the optimal positions for the fibre tips in a tumour, prior to an IPDT-treatment. It should be possible to integrate the algorithm into the IPDT-system developed at the Atomic Physics Department at the Lund Institute of Technology and SpectraCure AB. Demands on the algorithm is that it should be able to handle an arbitrary number of fibres in an arbitrarily shaped tumour geometry. In addition the optimization is supposed to be performed in connection with the treatment and the computation time is thus limited to a couple of minutes. The optimization goal is to minimize the treatment time and to spare surrounding sensitive tissues from receiving too high light doses.

This Master's Thesis starts with a theoretical background in the first three chapters; chapter 2 contains a description of photodynamic therapy, in chapter 3 the theory behind light propagation in scattering media is described and chapter 4 contains a description of the IPDT-system. Chapter 5 then deals with the different optimization algorithms that have been considered and/or tested and chapter 6 contains a short implementation description of the proposed algorithm. Then, in chapter 7, we describe the different algorithm tests that have been performed and their results. Finally, in chapter 8 and 9, the results are discussed, we present our conclusions and we give suggestions for future improvements.

2 Photodynamic therapy

Photodynamic therapy (PDT) is a non-thermal technique for local treatment of malignant tumours in which a substance called photosensitizer is administered to the body. The tissue under treatment is then illuminated with light of a specific wavelength, usually in the red wavelength region, and a photochemical reaction is induced as the photosensitizer absorbs the light. Most photosensitizers used in PDT have the characteristic to accumulate more in tumour tissue than in healthy tissue. This selectivity and the toxicity of the photochemical reaction, leading to local cell destruction, form the basis for this treatment. The presence of oxygen in the treated tissue is also important since oxygen is necessary for the photochemical reaction to take place [1,2].

2.1 Photosensitizers

There are three main criteria that a chemical compound must fulfil in order to be a good photosensitizer. First, it is essential that it accumulates to a higher degree in tumour tissue than in healthy tissue. Second, the photosensitizer must absorb light in a wavelength region for which the penetration depth in the surrounding tissue is rather good. Third, the photochemical reaction induced by the light absorption should efficiently kill the tumour cells.

A great number of compounds have been investigated in the search for the ideal photosensitizer. Traditionally, different porphyrin derivatives such as haematoporphyrin derivative (HpD) and Photofrin have been used as tumour seeking agents [2]. The chemical structure of the porphyrin main core is similar to the structure of the haem molecule except that it lacks the Fe ion in the centre (see Figure 2.1). The absorption spectrum of porphyrins has several peaks, the strongest around 405 nm (the Soret band) and several weaker ones at longer wavelengths up to 630 nm [2,3]. Usually light at around 630 nm is used since it penetrates tissue much better than shorter wavelengths.

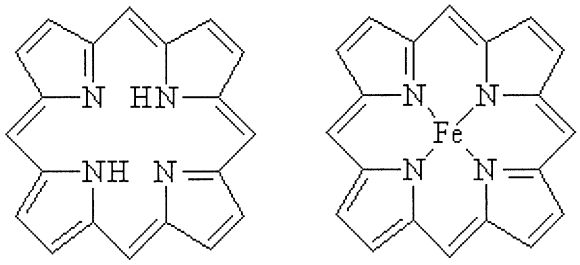

Figure 2.1 The main cores of the porphyrin and haem molecules.

The selective accumulation of porphyrins in tumour cells is due to numerous reasons e.g. lower pH and higher blood flow in tumour cells [3,4]. The accumulation may also be due to a difference in activity of important enzymes or better skin permeability in lesions, in the case of topically applied photosensitizers [5]. One of the main drawbacks of using Photofrin is the long lasting, extended skin photosensitivity of the patient, forcing him or her to avoid sunlight for several weeks or months after a treatment [2].

A different way to accumulate porphyrin in tumours is by administering the naturally occurring compound δ-aminolevulinic acid (ALA). This amino acid takes part in a chain of biochemical reactions called the haem-cycle wherein it is converted to the photodynamically active Protoporphyrin IX (PpIX) [2] (see Figure 2.2). In the synthesis of haem the first step is the formation of ALA from glycine and succinyl co-enzyme A. This step is self regulated by the concentration of haem. The following steps leading to the formation of PpIX are quite rapid and not rate-limiting. The last step involving the incorporation of a Fe^{2+} ion in the PpIX molecule to form haem is a rather slow process. When supplying ALA in excess, the self-regulatory system is overloaded and porphyrins are accumulated due to their slow conversion into haem [3,6]. Since this process occurs to a higher degree in tumour cells and since Protoporphyrin IX is photodynamically active it is then suitable to perform PDT. The main advantages of ALA compared to other photosensitizers are that it is naturally occurring and thereby low-toxic and that it has a high clearance rate, i.e. most of the substance is transferred to haem within one or two days and no long lasting extended skin photosensitivity is experienced by the patient [2,3]. Today ALA is one of the most commonly used photosensitizers for PDT. It can be given topically, orally or by intravenous injection.

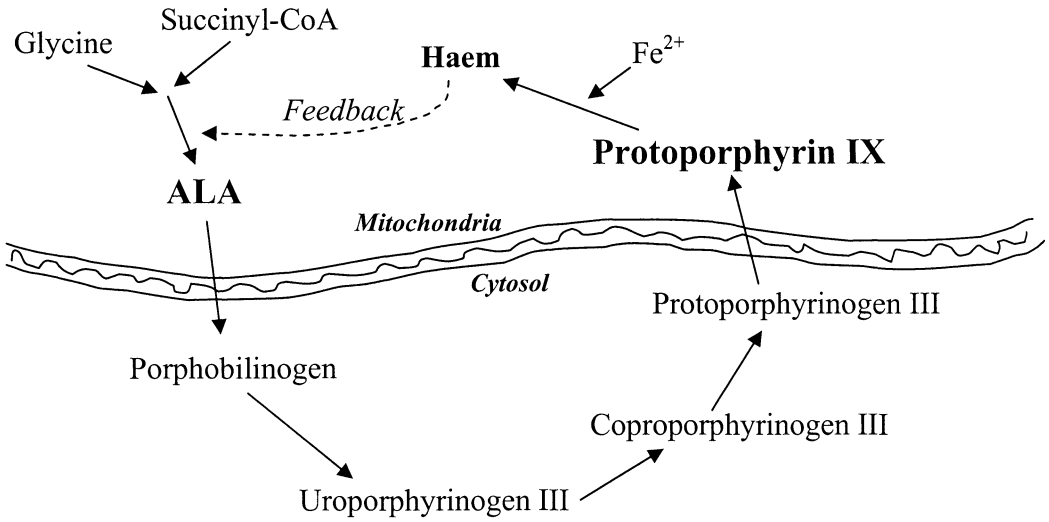

Figure 2.2 The synthesis of haem takes place partly in the mitochondria and partly in the cytosol. A supply of extra ALA causes an accumulation of the photodynamically active substance Protoporpfyrin IX.

The search for new and even better photosensitizers proceeds all the time. Desired characteristics of new sensitizers are improved selectivity for tumours and light absorption at higher wavelengths, closer to infrared, where the penetration depth is larger. Other types of molecules being investigated are e.g. chlorines, phtalocyanines and texaphyrins [2].

2.2 Mechanisms of PDT

As previously mentioned, the treatment of a tumour using PDT requires the selective accumulation of a photosensitizer in the tumour cells, the subsequent light exposure and the presence of oxygen. The photodynamic process is based on the optical excitation of the photosensitizer and a following transfer of energy to nearby molecules.

When a porphyrin is used as photosensitizer the photodynamical process starts with the absorbance of light with a wavelength of about 630 nm. This will cause an excitation of the molecules to the first excited singlet state (S_1), also called the Q-band (see Figure 2.3). From here the molecules can relax back to the ground state (S_0) under the emission of fluorescence light. Since the photosensitizer is tumour-seeking this light can be used as a diagnostic tool [1]. Another alternative is that the molecules in the S_1-state relax to the first triplet state (T_1). This transfer is spin-forbidden but can occur with a rather high probability anyway because of the small energy separation between the states. From the T_1-state the relaxation back to the ground state is again a spin-forbidden process which makes the T_1-state a metastable state, i.e. with a relatively long lifetime. This leads to a high probability for interaction with surrounding molecules [2].

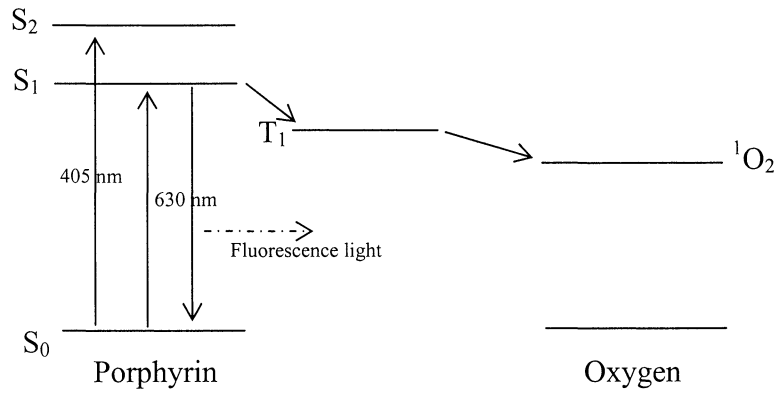

Figure 2.3 Energy level diagram showing the photodynamic process with the transfer of energy from porphyrin to oxygen. An excitation to the S2-state occurs when the porphyrin absorbs light in the Soret band (405 nm).

There are two different reactions of interest for PDT that can occur. In the first (type I), energy from the excited triplet state (T_1) of the sensitizer is transferred to another molecule via electron transfer or hydrogen abstraction [2,3]. This causes the formation of reactive radicals often involving oxygen [1]. In the second and most important reaction (type II), energy is transferred to molecular oxygen causing an excitation to one of the first singlet states. Singlet oxygen ($^1O_2$) is very reactive and acts as an aggressive oxidant of e.g. proteins, nucleic acids and phospholipids. Because of the high reactivity the diffusion length of $^1O_2$ in biological tissue is very short and the caused damage is thus very limited in range. This short radius of action and the selective accumulation of the photosensitizer in tumour tissue will spare surrounding tissue from severe damage [2,3].

During the treatment the oxygen is consumed causing a decrease in oxy-haemoglobin and an increase in deoxy-haemoglobin. The oxygen saturation level SO_2, defined as:

$$S_{o_2} = \frac{[HbO_2]}{[Hb]+[HbO_2]} \qquad \text{(Eq. 2.1)}$$

will thus decrease during the treatment. [HbO_2] and [Hb] denotes oxy- and deoxy-haemoglobin, respectively.

The fluorescence declines rapidly when the treatment is started, a phenomenon called photobleaching or photodegradation. Since singlet oxygen is generated in the sensitizer's immediate surroundings there is a risk that it will oxidize the sensitizer instead of the intended cell organelles. Unfortunately the sensitizer is consumed when photobleached and can thus not be used to generate new singlet oxygen molecules. In spite of the consumption a high degree of photobleaching seems to be a good thing because it is a sign of good access to oxygen. Results have been found showing a correlation between treatment outcome and the initial photobleaching rate [7].

2.3 Treatment considerations

The result of a PDT treatment is dependent on the three parameters: the dose of the sensitizer in the tumour tissue, the amount of delivered light of the appropriate wavelength and the availability of oxygen. The product of light dose and sensitizer concentration should reach above the threshold for necrosis in the tumour whereas the effect in surrounding healthy tissue should be below this threshold [1].

With a good photosensitizer and a restrictive light delivery system a high selectivity for tumour necrosis can be achieved, which is a great advantage compared to conventional treatment modalities. Other advantages of PDT are the use of non-ionizing radiation, minimizing long-term side-effects and allowing repeated treatment sessions, and the good cosmetic results due to smooth scar formation [1,8].

Up to now PDT has mostly been used to treat superficial tumours by illuminating the skin of the patients. In these treatments it has been possible to apply the photosensitizer topically. A drawback of this method can be a non-uniform distribution of the sensitizer in the tumour, resulting in poor treatment results for deeper-lying parts [9]. This can be avoided through oral or intravenous administration of the photosensitizer. But, then the drug dose has to be increased and the whole body is exposed which might lead to light sickness feelings or extended skin photosensitivity for certain sensitizers, such as Photofrin [2].

2.4 Interstitial PDT

The main drawback of PDT is generally the relatively low penetration depth of the light in biological tissue. This has so far been a very limiting factor considering the type of tumours that can be treated. Under development is therefore now the technique of interstitial photodynamic therapy (IPDT) involving the light delivery through optical fibres inserted into the tumour mass. This technique will allow the treatment of thicker and/or deeper-lying tumours. See chapter 4 "the IPDT-system" for more information about IPDT.

3 The interaction of light with tissue

When light, or electromagnetic radiation in general, interacts with tissue, different processes can occur. The light may be transmitted, reflected, absorbed, scattered or re-emitted. What happens is strongly dependent on the wavelength of the radiation. High energy radiation such as gamma- or X-rays is not scattered to a large extent but rather penetrates the tissue in straight trajectories. This type of radiation is attenuated due to absorption that varies in different kind of tissue and it can thus be used for imaging such as ordinary X-ray images. When absorbed, however, high energy radiation can have ionizing or bond breaking effects on molecules, effects that may be carcinogenic. Low-energy radiation such as far IR- or microwave radiation, on the other hand, can excite vibrational- and rotational levels in molecules leading to a temperature increase in the tissue [2]. Suitable for medical laser treatment is therefore the wavelength region reaching from UV to near IR, including the visible region situated between approximately 400 and 700 nm (see Figure 3.1).

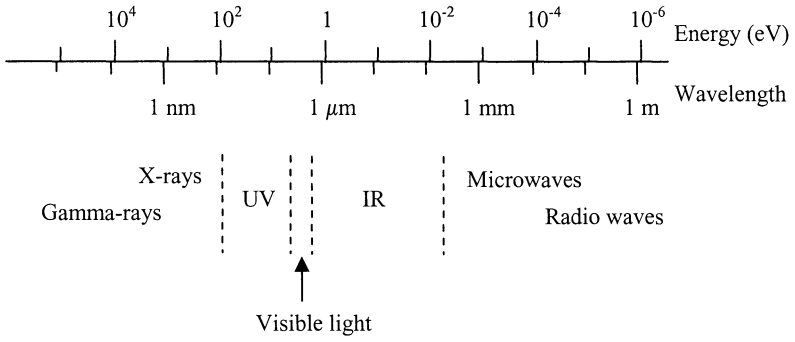

Figure 3.1 The spectrum of electromagnetic radiation.

When light is sent towards biological tissue a small part of it may be reflected at the tissue surface. The amount of reflected light depends on the angle of incidence and the refractive index of the tissue, which is normally 1.35-1.45 [2]. Most of the light will normally enter though, and in the tissue it may then be absorbed or scattered. Both of these processes, which are described in greater detail below, are strongly wavelength dependent.

3.1 Absorption

A photon may be absorbed by a molecule in the tissue if the energy of the photon corresponds to the energy gap between two electronic states in the molecule. This explains the wavelength dependency of the absorption. Particles in the tissue that absorb light are called chromophores. Important chromophores in the visible and near-IR region are e.g. haemoglobin and melanin. Water, present in most tissue types, is also an important absorber, especially above 1300 nm and below 200 nm.

In the lower wavelength part of the visible spectrum the probability for absorption is about the same as for scattering whereas in the red and near-IR region the absorption probability is much lower and the light penetrates the tissue better. This wavelength region is therefore called the optical window [8] (see Figure 3.2).

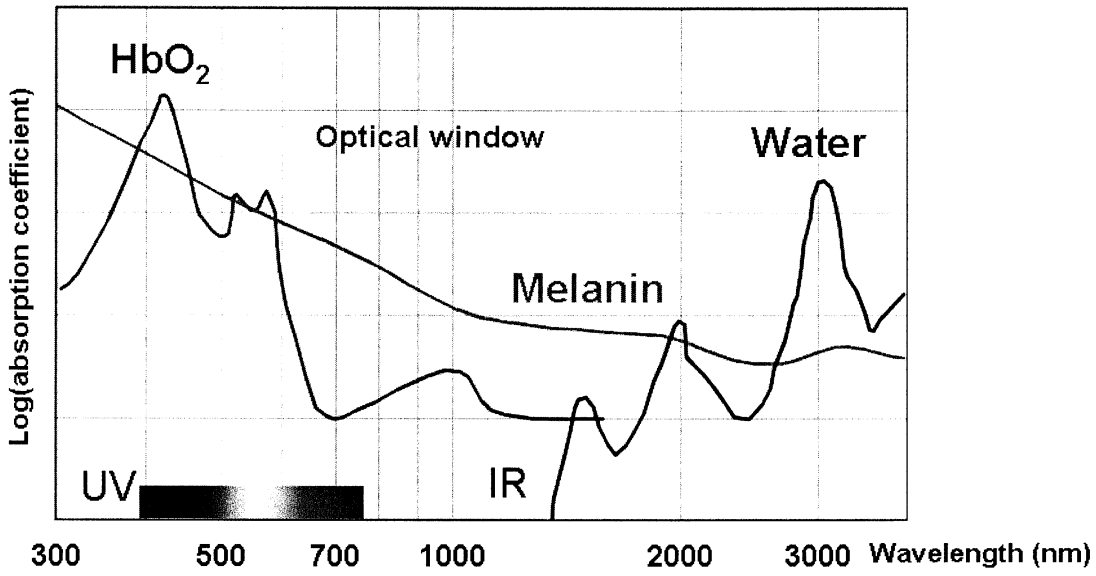

Figure 3.2 Absorption spectrum for oxy-haemoglobin, melanin and water. Indicated are also the visible light region and the wavelength region called the optical window [10].

The physical parameter used to describe the absorption of light in tissue at a given wavelength is the absorption coefficient, μ_a. It is defined as the probability of absorption per unit length and is often given in mm^{-1} or cm^{-1}.

The energy absorbed by a molecule in tissue may be re-emitted as fluorescence or induce a photochemical reaction. It might also be redistributed to nearby molecules in the form of heat inducing a rise in temperature in the tissue [1,2,5].

3.2 Scattering

The different scattering processes that can occur in tissue can be divided into two main groups; elastic and non-elastic scattering. Elastic scattering means that the photon is scattered without any change in energy (wavelength) whereas non-elastic scattering means that the scattered photon has a lower or higher energy than the incoming. Elastic scattering involving particles with a size much smaller than the wavelength of the light, such as free atoms and molecules, is called Rayleigh scattering. When the scattering object is larger than the wavelength of the incident light, it is called Mie scattering.

The wavelength dependency for scattering is not as important as for absorption but still it is approximately λ^{-1}-λ^{-2} for larger particles (Mie scattering) and λ^{-4} for smaller particles

(Rayleigh scattering). This means that blue light is more scattered than red light since it has a shorter wavelength [2,5]. Scattering in tissue is a very complex process which can be described as a mixture of Mie and Rayleigh. Measured values of the wavelength dependency for tissue are usually close to λ^{-1} [4].

In analogy with the absorption coefficient, the probability of scattering per unit length is described by the scattering coefficient, μ_s (cm^{-1}). The total attenuation coefficient, μ_t is the sum of μ_a and μ_s and describes thus the total probability of interaction per unit length.

3.3 Anisotropy

Scattering in a turbid medium, such as biological tissue, is not isotropic. Incident light is much more likely to be scattered forwards than backwards and the scattering is therefore said to be forward directed. The scattering anisotropy is normally described by the so called g-factor. It is defined as the mean cosine of the scattering angle. The value of g can vary between -1 and +1, where g = -1 means total backscattering, g = 0 means isotropic scattering and g = +1 means total forward scattering [1] (see Figure 3.3).

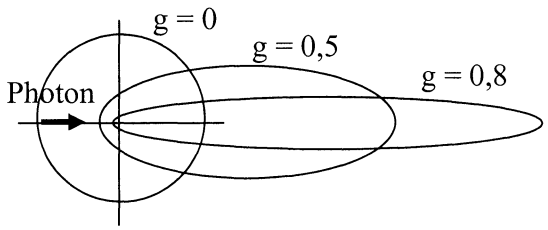

Figure 3.3 The scattering phase function for different g-values.

A very useful unit in tissue optics is the reduced scattering coefficient, μ_s' defined as:

$$\mu_s' = \mu_s(1-g)$$

This parameter describes the effective mean free path between two scattering events assuming that all scattering events are isotropic, i.e. g = 0. It can thus be interpreted as the inverse of the mean distance a photon travels before the total scattering can be considered isotropic [5].

3.4 Transport equation

To describe light transport in tissue, transport theory has proven useful. The basic idea of transport theory is to describe an energy balance in an infinitesimal volume. Considered are incoming, outgoing, absorbed and emitted energy, in this case in the form of photons. Mathematically this is described by a differential equation called the transport equation, which will be derived below.

The distribution of light, as a function of position in space, $\boldsymbol{r}$, direction, $\boldsymbol{\Omega}$, and time, t, can be expressed as a single-particle distribution function: $N(\boldsymbol{r},\boldsymbol{\Omega},t)$, with the unit $m^{-3}sr^{-1}$. Since all photons travel with the same speed $v = c/n$, where c is the speed of light in vacuum and n is the refractive index of the medium, only the so-called one speed case will be considered here. The radiance or intensity of the light, $L(\boldsymbol{r},\boldsymbol{\Omega},t)$, is obtained by multiplying N by the speed v, and the energy of the photons, hc. Radiance is the quantity used to describe the propagation of photon power and the unit is thus $Wm^{-2}sr^{-1}$. The density of photons $\rho(\boldsymbol{r},t)$ is given by the integral of N over all possible directions [1,2]:

$$\rho(\boldsymbol{r},t) = \int_{4\pi} N(\boldsymbol{r},\boldsymbol{\Omega},t)d\Omega$$

The photon current density $\boldsymbol{J}(\boldsymbol{r},t)$ is given by the integral of $v\boldsymbol{\Omega}N$ over all directions:

$$\boldsymbol{J}(\boldsymbol{r},t) = v\int_{4\pi} \boldsymbol{\Omega}N(\boldsymbol{r},\boldsymbol{\Omega},t)d\Omega$$

Another quantity of interest for practical use is the fluence rate $\phi(\boldsymbol{r},t)$ [Wm^{-2}]. It is defined as the radiant power incident on a small sphere, divided by the cross-sectional area of that sphere. Fluence rate is expressed as:

$$\varphi(\boldsymbol{r},t) = \int_{4\pi} L(\boldsymbol{r},\boldsymbol{\Omega},t)d\Omega$$

A simple way to derive the transport equation is to start from the balance equation for the conservation of particles traveling in a defined direction $\boldsymbol{\Omega}$ in an infinitesimal volume element V (see Figure 3.4). This balance equation can be written as:

dN = - photons lost through the boundary (a)
- photons absorbed within the volume V (b)
- photons scattered from the direction $\boldsymbol{\Omega}$ into any other direction $\boldsymbol{\Omega}'$ (c)
+ photons scattered from any direction $\boldsymbol{\Omega}'$ into the direction $\boldsymbol{\Omega}$ (d)
+ photons produced from light sources within V (e)

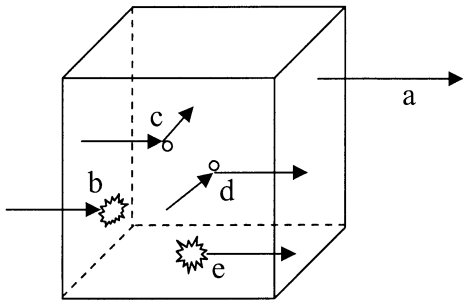

Figure 3.4 A schematic representation of the balance equation used to derive the transport equation.

Mathematically the basic transport equation for light propagation in tissue can be written as [1]:

$$\int_V \frac{\delta N(\boldsymbol{r},\boldsymbol{\Omega},t)}{\delta t} dV = -\int_V v\boldsymbol{\Omega}\cdot\nabla N(\boldsymbol{r},\boldsymbol{\Omega},t)dV \ (a) \quad -\int_V v\mu_a(\boldsymbol{r})N(\boldsymbol{r},\boldsymbol{\Omega},t)dV \ (b)$$
$$-\int_V v\mu_s(\boldsymbol{r})N(\boldsymbol{r},\boldsymbol{\Omega},t)dV \ (c)$$
$$+\int_V v\mu_s(\boldsymbol{r})\int_{4\pi} p(\boldsymbol{\Omega}'\cdot\boldsymbol{\Omega})N(\boldsymbol{r},\boldsymbol{\Omega}',t)d\Omega' dV \ (d) \quad +\int_V q(\boldsymbol{r},\boldsymbol{\Omega},t)dV \ (e)$$

Since all terms are integrated over an arbitrary volume V the equality must also be valid for the integrands. Using that $\mu_a + \mu_s = \mu_t$ then yields the simplified transport equation:

$$\frac{\delta N(\boldsymbol{r},\boldsymbol{\Omega},t)}{\delta t} = -v\boldsymbol{\Omega}\cdot\nabla N(\boldsymbol{r},\boldsymbol{\Omega},t) - v\mu_t(\boldsymbol{r})N(\boldsymbol{r},\boldsymbol{\Omega},t)$$
$$+ v\mu_s(\boldsymbol{r})\int_{4\pi} p(\boldsymbol{\Omega}'\cdot\boldsymbol{\Omega})N(\boldsymbol{r},\boldsymbol{\Omega}',t)d\Omega' + q(\boldsymbol{r},\boldsymbol{\Omega},t)$$

Different methods can be used to solve the transport equation. Common for all methods is that some sort of simplification is used [1]. For the case of light propagation in tissue one very useful approach is the diffusion approximation.

3.5 Diffusion approximation

The first step in the diffusion approximation is an expansion of the functions in the transport equation into spherical harmonics. In this way the photon distribution function $N(\boldsymbol{r},\boldsymbol{\Omega},t)$ can be written:

$$N(\boldsymbol{r},\boldsymbol{\Omega},t) = \sum_{l=0}^{\infty}\sum_{m=-l}^{+l}\sqrt{\frac{2l+1}{4\pi}}N_{lm}(\boldsymbol{r},t)Y_{lm}(\boldsymbol{\Omega})$$

The source function $q(\boldsymbol{r},\boldsymbol{\Omega},t)$ and the phase function $p(\boldsymbol{\Omega}'\cdot\boldsymbol{\Omega})$ can be expanded in the same way. This results in an infinite series of coupled differential equations. To reach a solution this series must be truncated at some l. The lowest order approximation, where only the terms for which $l = 0$ or $l = 1$ are kept, is called the P_1-approximation or the diffusion approximation. For the distribution function this yields:

$$N(\boldsymbol{r},\boldsymbol{\Omega},t) = \sqrt{\frac{1}{4\pi}}N_{00}(\boldsymbol{r})Y_{00}(\boldsymbol{\Omega}) + \sqrt{\frac{3}{4\pi}}\sum_{m=-1}^{1}N_{1m}(\boldsymbol{r})Y_{1m}(\boldsymbol{\Omega})$$

Noticing that Y_{00} is a scalar and Y_{1m} is a vector (with the three elements m = -1, 0, +1) we can write the distribution function as:

$$N(\boldsymbol{r},\boldsymbol{\Omega},t) = A + \boldsymbol{\Omega}\cdot\boldsymbol{B}$$

Integrating this equation over Ω gives A and a multiplication of the equation by Ω followed by an integration over Ω gives $\boldsymbol{B}$:

$$A = \frac{1}{4\pi}\rho(\boldsymbol{r},t) \qquad\qquad \boldsymbol{B} = \frac{3}{4\pi v}\boldsymbol{J}(\boldsymbol{r},t)$$

The photon distribution function can now be written:

$$N(\boldsymbol{r},\boldsymbol{\Omega},t) = \frac{1}{4\pi}\left[\rho(\boldsymbol{r},t) + \frac{3}{v}\boldsymbol{J}(\boldsymbol{r},t)\cdot\boldsymbol{\Omega}\right]$$

where $\rho(\boldsymbol{r},t)$ and $\boldsymbol{J}(\boldsymbol{r},t)$ are the photon density and the photon current density respectively, as stated above. In a similar way the source function can be written as:

$$q(\boldsymbol{r},\boldsymbol{\Omega},t) = \frac{1}{4\pi}\left[q_0(\boldsymbol{r},t) + 3\boldsymbol{q}_1(\boldsymbol{r},t)\cdot\boldsymbol{\Omega}\right]$$

Inserting these two equations in the transport equation the integral can be solved. Further mathematical simplifications of the resulting expression and integration over all directions then yield:

$$\frac{1}{v}\frac{\delta\rho}{\delta t} = -\mu_a\rho - \frac{1}{v}\nabla\cdot\boldsymbol{J} + \frac{1}{v}q_0$$

Using *Fick's law* ($\boldsymbol{J} = -vD\nabla\rho$) the final diffusion equation can then be written as:

$$\frac{1}{v}\frac{\delta\rho}{\delta t} - \nabla^2 D\rho + \mu_a\rho = \frac{1}{v}q_0 \qquad \textit{where} \quad D = \frac{1}{3(\mu_a + (1-g)\mu_s)}$$

Since the fluence rate and the photon density are related by $\varphi = chv\rho$ the diffusion equation can equally be expressed for the fluence rate as:

$$\frac{1}{v}\frac{\delta\varphi}{\delta t} - \nabla^2 D\varphi + \mu_a\varphi = \frac{1}{v}q_0$$

For an even more thorough description of the derivation of the transport- and diffusion equations see e.g. [1] or [2].

Interesting for our work has been the steady state (no time dependence) case of the diffusion equation that can be expressed:

$$\nabla^2 D\varphi(r) - \mu_{eff}\varphi(r) = Q(r) \qquad where \quad \mu_{eff} = \sqrt{3\mu_a(\mu_a + \mu_s(1-g))}$$

The solution for a point source in an infinite homogeneous medium can be written as:

$$\varphi(\boldsymbol{r}) = \frac{P\mu_{eff}^2}{4\pi\mu_a}\frac{1}{|\boldsymbol{r}|}e^{-\mu_{eff}\cdot|r|} \qquad \text{(Eq. 3.1)}$$

This equation has been used to calculate the light distribution in tissue when light is sent in through an optical fibre [5]. Hence, this is the expression for the fluence rate used in this work. *P* represents the power emitted from the tip of the fibre.

Various numerical methods, such as Monte Carlo simulation and the adding doubling method, can also be used to calculate the light distribution in tissue.

3.6 Tissue optical properties

Biological tissue is highly inhomogeneous. As mentioned earlier the absorption is strongly wavelength dependent. In our work we have assumed laser light of 635 nm since that is the wavelength used in the current version of the IPDT-system. At this wavelength the absorption coefficient μ_a in soft tissue is approximately in the order of 0.01 mm^{-1} [8].

The wavelength dependency for scattering is not as strong as for absorption. The scattering normally decreases smoothly with wavelength. At 635 nm the scattering coefficient μ_s in soft tissue is approximately in the order of 10 mm^{-1}. As mentioned before tissue is highly forward scattering and a typical value of g at 635 nm in soft tissue is 0,9. Hence, the value of the reduced scattering coefficient μ_s' is usually in the order of 1 mm^{-1} [8].

One way to compensate for the strong forward scattering in tissue and to simplify the calculations is to introduce the parameter $z_0 = 1/\mu_s'$ [11]. We can assume that all photons are initially scattered at this depth from the fibre tip. At this depth we can thus assume an isotropic light source.

3.7 Theoretical assumptions

To simplify our work to develop an optimization algorithm for the fibre placement in an arbitrarily shaped tumour we have made a few assumptions. First of all there are certain restrictions for the diffusion equation.

The diffusion equation is only valid for the case of diffuse light which implies that the reduced scattering coefficient in the medium must be much larger than the absorption coefficient, i.e. $(1\text{-}g)\mu_s >> \mu_a$. In addition, the separation between the source and the detection point has to be large (≥ 2 mm). This restriction also guarantees diffuse light at the detection point. In our work we have assumed the diffusion equation to be valid in all parts of the geometry.

Further on, we assume an approximately homogenous medium regarding the optical properties μ_a, μ_s and g, i.e. we assume that the probability for absorption and scattering respectively are more or less the same in different parts of the tumour. In addition we do not take into account different boundary effects such as reflection.

Finally, for simplicity, we also assume that a fibre does not disturb the fluence field from another fibre.

4 The IPDT-System

4.1 Technical description[1]

The IPDT-system can not only deliver therapeutic light but also carry out optical measurements using the same optical fibres. By doing these measurements it is possible to monitor the treatment progression.

A schematic picture over the system can be seen in Figure 4.1. As seen the system consists of two main parts; the optical unit, which delivers and receives light, and a laptop computer that controls the system. The optical unit can in turn be divided into four different parts: Therapeutic light unit, Measurement light unit, Spectrometer and Light distribution module.

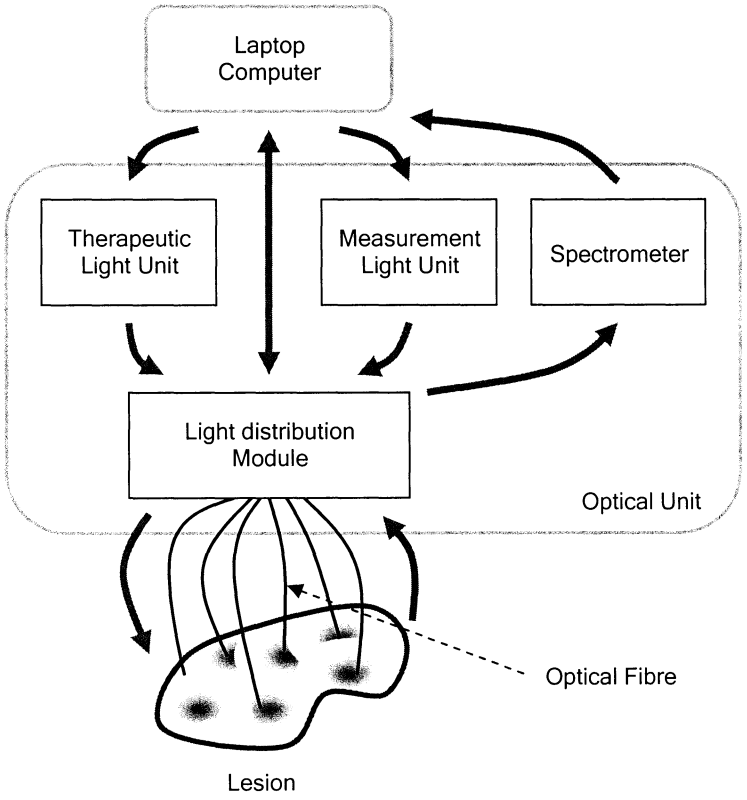

Figure 4.1. A flow chart describing the IPDT-system. The arrows between the laptop computer and other instruments represent digital information and rest of the arrows represents information in the form of light.

The whole system is controlled by the laptop using a program implemented in LabView™ (National Instruments, Austin, USA).

[1] Based on [12].

The light distribution module constitutes the heart of the optical unit since it determines whether the system is running in therapeutic or in measuring mode. The main part is a rotunda consisting of two metal discs placed closely together facing each other (see Figure 4.2). The first disc has 12 fibre connectors and is fixed; the second disc has 6 fibre connectors and can rotate around the common axis. All the fibre connectors are placed at the same distance from the disc's center and are separated by 30 and 60 degrees respectively. Six connectors of disc 1 will every 30 degrees overlap the turnable disc's 6 connectors. When two connectors overlap light can be transmitted between the two in a highly efficient way.

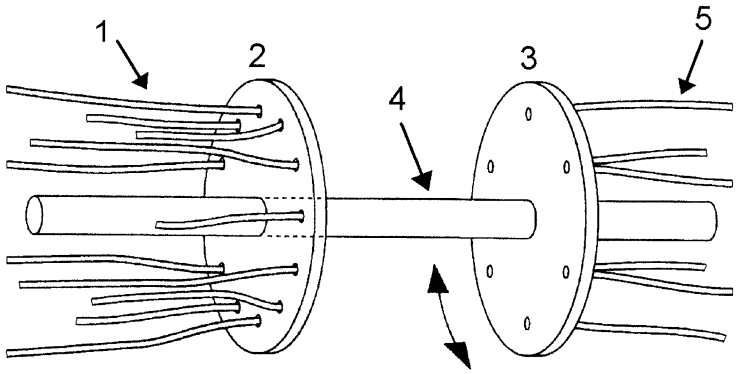

Figure 4.2. Showing the rotunda with the discs separated. The fixed disc is marked by number 2 and the turnable disc (3) can rotate around the common axis (4). The 12 fibres that are attached to the fixed disc are marked by number 1 and the 6 patient fibres, connected to the turnable disc, by number 5 [13].

Six diode lasers are connected via six 100 μm optical fibres to every other connector at the fixed disc. Maximum output power from the diode lasers altogether is about 1.2 W. The six remaining connectors on the fixed disc are used by the measurement unit; five of them guide the light from the beam-coupling unit and into the spectrometer and the twelfth fibre couples light from one of the two measurement light sources into one of the patient fibres. Six optical fibres with a core diameter of 400 μm are attached to the connectors of the tuneable disc. These are called patient fibres because they deliver light into the patient during treatment.

If the turnable disc is orientated so that its connectors face the fibres from the diode lasers the system is said to be in therapeutic mode and if they face the spectrometer fibres and the measurement light source fibre the system is in measurement mode. When the system is in measurement mode and the turnable disc is rotated 60 degrees it will remain in measurement mode but another patient fibre will be delivering light from the measurement light unit.

When changing from treatment to measurement mode the turnable disc is turned 30 degrees. The six patient fibres will now be connected to the five fibres attached to the spectrometer and one fibre will be connected to one of the light sources (see Figure 4.3).

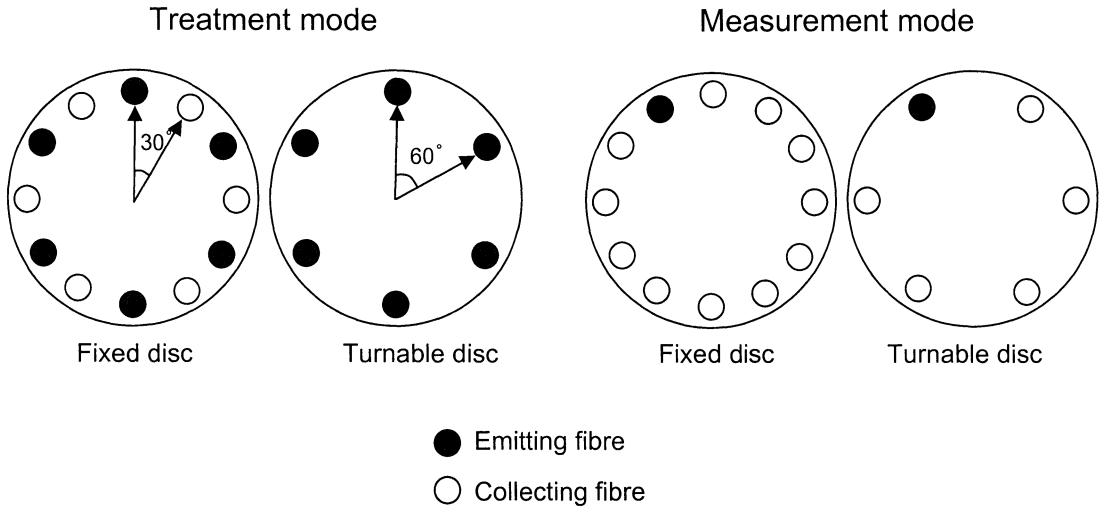

Figure 4.3. Schematic picture showing how the discs are orientated relative to each other in treatment and measurement mode respectively.

Light coming from one of the measurement light sources and delivered through one of the patient fibres interacts with the tissue and the resulting light is collected by the other five fibres. After passing through the rotunda the light enters the spectrometer and five spectra are recorded. Using a separate beam-coupler, light from two measurement light sources is successively coupled into the active fibre. The first source is a diode laser emitting light at 635 nm, the second source is the IR light-emitting diode and the third (not yet implemented) can be a laser emitting light at 405 nm. The same measurements are performed letting each of the patient fibres be the emitting fibre whereas the rest act as collecting fibres. This measurement procedure is performed by rotating the turnable disc 60 degrees five times.

4.2 Treatment procedure

In order to always achieve good treatment results a certain treatment procedure is followed. The procedure consists of three main parts:

- Dosimetry planning
- Fibre insertion
- The treatment

4.2.1 Dosimetry planning

The first step in the dosimetry planning is to define what part of the tissue that is tumour and what is not. A step in doing this is to get some sort of picture of the tissue. Two possible techniques for doing this are ultrasound and magnetic resonance imaging (MRI). Since the two techniques are based on measuring different physical properties you can not expect them to give exactly the same result. The advantage using ultrasound is that it can be performed in the operating theatre just before the treatment starts. The main drawback is the low resolution for deep lying tumours. MRI-images have a high resolution but the disadvantage is that this procedure must be performed prior to the treatment occasion. The expensive MRI-machines will thus imply higher medical costs and be more inconvenient for the patient.

Secondly you have to determine where to place your patient fibres. This is where our optimization algorithms come in. Placing the fibres by hand is not a good thing to do if you want to minimize the treatment time since this is really hard to do in a 3D-picture (See chapter 7.1 and 8.1).

The third and last step in the dosimetry planning is the actual dose calculations. These are performed using the finite element method (FEM) to solve the diffusion equation (see chapter 3.5) for the specific fibre positions and tumour geometry. The dose calculations result in a preliminary treatment time. The actual treatment time will probably differ from the calculated one since the optical properties of the specific patient's tumour are not known and certain changes are induced during the treatment (see chapter 4.3).

4.2.2 Fibre insertion

Inserting optical fibres into a patient and placing the tips with mm-precision is not an easy thing to do. The fibres are both fragile and flexible and the tissue tends to move around during the insertion. By inserting a hollow needle, which is much more rigid, with an optical fibre placed in its inner bore, you can both protect the fibre and place it with a higher precision. The main drawback in using needles for insertion is that they are thicker than the optical fibres, allowing the fibre to be placed in its centre. A needle with too thin walls will not be rigid enough to allow any high precision placements. By using rigid needles it should be possible to place the fibres within a location of a couple of mm from the ideal position [14].

To ease the needle insertion a template, shaped as a two dimensional grid, can be fixated outside the body (see Figure 4.4). The template ensures that all the needles will be inserted from the same direction. If you then know how the template coordinate system and the picture coordinate system, which is given by the axes orientation in e.g. the MRI-image of the tumour, relate to each other, it is possible to convert the fibre coordinates in the picture coordinate system to coordinates in the template coordinate system. One way of determining the relation between the two coordinate systems is to fixate the grid to the patient before the MRI-image is taken. By doing this you can see the template in the image and get its orientation relative the image coordinate system.

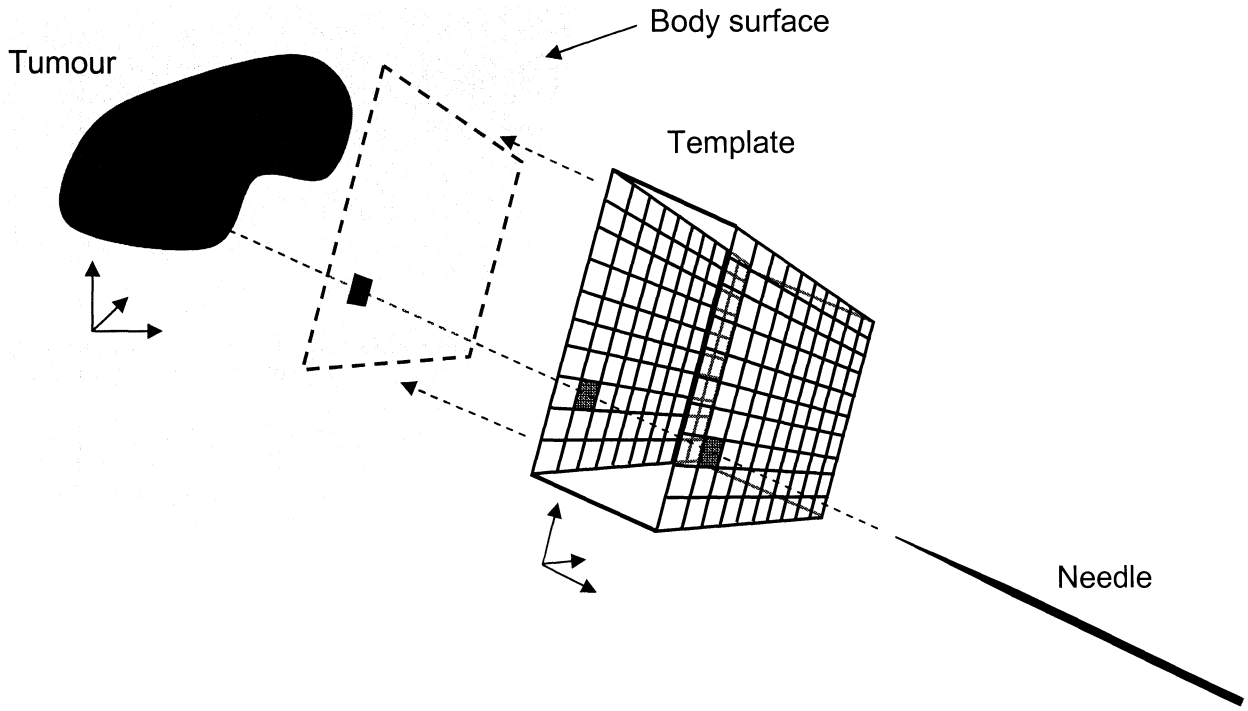

Figure 4.4. Illustrates the idea of using a 2D-grid to align all the needles during insertion.

Most often the tissues will move around when you insert the needles. Attempts have been made to fixate the disobedient tissue using retractable barb [14]. This will of course facilitate the fibre placement but the barb will at the same time cause tissue damage. A damaged tissue can cause a haemorrhage (bleeding) which will lead to reduced fluence rate in parts of the tumour during treatment. If a fibre tip is surrounded by blood most of the light emitted from it will be absorbed by the blood causing generation of heat and even blood coagulation.

If you accept the fact that the tissues might move around a little during the fibre insertion you can instead observe the movements and try to compensate for it using ultrasound as guidance. When all the fibres are inserted the chance that they are placed exactly where you want them to be is minimal. To get revised information about the treatment time a new dose calculation can be performed, this time using the actual coordinates of the fibre tips.

4.2.3 The treatment

The next step is to perform the treatment. What makes the IPDT-system special is its ability to measure fluence rate, sensitizer fluorescence and oxygen concentration during the treatment. This allows you to monitor the treatment progression and adapt the

treatment to the physical conditions and optical properties at the specific treatment. The monitoring measurements are not done continuously during the treatment so the treatment must temporarily be stopped when a measurement is to be made. The system is said to be running in either treatment or measurement mode. The measurement sequence takes approximately 45 s and is performed with 30 up to 120 s time intervals [12]. The treatment continues by repeatedly changing between treatment and measurement mode until the desired dose is reached.

4.3 Input and output parameters

As said earlier three parameters are repeatedly measured during the treatment: light fluence rate, sensitizer fluorescence intensity and the change in local tissue oxygen saturation level.

4.3.1 Measuring the light fluence rate

The first step in the measurement cycle is to measure the light transmission from one fibre to rest of the fibres. When repeatedly measuring the fluence rate during treatments it is possible to monitor the treatment progression and reveal bleedings, blood coagulations and treatment induced changes in light transmission. The measurement constitutes a necessary feedback to prevent insufficient treatment. In (13) it was studied how the light transmission changes during the treatment. The results can be seen in Figure 4.5 below.

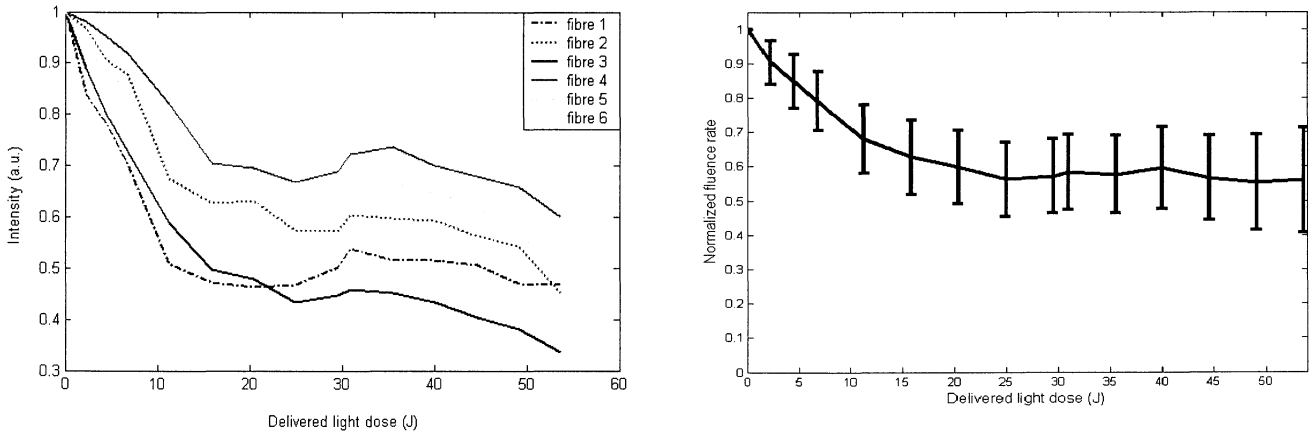

Figure 4.5. The first plot shows the detected fluence rate at five fibres when the light is delivered by the sixth fibre ('fibre 5') as a function of delivered dose. Plot number 2 shows the average fluence rate as a function of delivered dose. The data are received from one treatment and are normalized with respect to the first measurement, which is done before the treatment is started. Plot number 2 is thus an average of 30 plots. In the plot the uncertainty is indicated by plotting 1 SD above and one below the average data (13).

When looking at Figure 4.5 it is quite obvious that the light transmission tends to decrease during the treatment. This decrease seems not to be a result of one single factor but rather a result of several biological changes induced by the treatment. Considered factors are:

- Increased blood flow in the tumour area
- Change in oxygen saturation level [15]
- Induced damage to tissue microcirculation [16]

PDT-treatment induces a swelling in the treated tissue area. If the swelling is a result of tissue irritation you could assume that the blood flow has increased, causing the tissue to swell. Since blood is one of the major absorbers in the tissue optical window an increase of blood will cause a decrease in light transmission.

During the treatment, the oxygen saturation level SO_2, defined in Eq. 2.1, will decrease. Since deoxy-haemoglobin is a stronger absorber of light at 635 nm compared to oxy-haemoglobin (see Figure 4.7A) a decrease in the tissues oxygen saturation level will also cause a decrease in light transmittance in the tissue.

The third possible contributory factor is the damage to tissue microcirculation caused by the treatment. The smallest blood vessels are also the most sensitive ones. When the singlet oxygen oxidizes the walls of the smallest blood vessels, they can burst. Blood will then exit the vessels and enter the space between cells. If this happens the blood will no longer be concentrated to vessels but be more homogenously distributed in the tissue. The scattered laser light will then more often pass through areas containing the highly absorbing blood and the transmittance will thereby decrease.

4.3.2 Measuring the sensitizer fluorescence intensity

The second parameter the system repeatedly measures is the sensitizer fluorescence intensity. The sensitizer is excited using the same diode laser used during the fluence rate measurements, which emits light at 635 nm. The fluorescence is measured at 705 nm where PpIX has a fluorescence peak, see Figure 4.6B. An example of how the average fluorescence proceeds during a PDT-treatment can be seen in Figure 4.6A. The fluorescence detected in each fibre is first normalized with respect to its initial value and then the mean of the 30 measurements is calculated. No compensation for the increased absorption has been made.

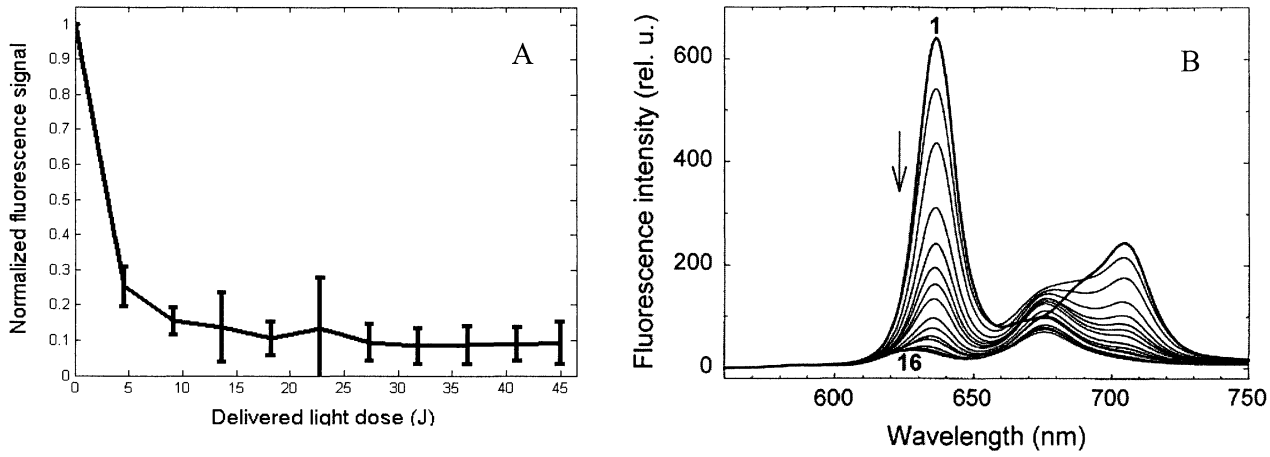

Figure 4.6. The first figure shows how the fluorescence in average changes during the treatment. The plot is an average of 30 normalized fluorescence signals here shown with error bars denoting 1 SD. In the second figure a fluorescence emission spectrum from ALA-induced protoporphyrin IX (PpIX) in normal mouse skin is shown [17]. The thick line represents the fluorescence before light exposure from a 100 mW/cm^2 laser. The narrower lines shows the fluorescence after an exposure time of 0.5, 1, 2, 3, 4, 5, 6, 8, 10, 12.5, 15, 20, 25, 30 and 40 minutes. Photobleaching (photodegradation) is mainly responsible for the decline in PpIX concentration and thus the change in fluorescence.

4.3.3 Measuring the oxygen saturation level, SO_2

To retrieve the oxygen saturation level SO_2 the fluence rate from one fibre to all other are recorded at 760 and 800 nm using the NIR LED. At 800 nm oxy- and deoxy-haemoglobin absorbs equally much but not at 760 nm (see Figure 4.7B), a fact that is utilized when calculating the oxygen saturation level.

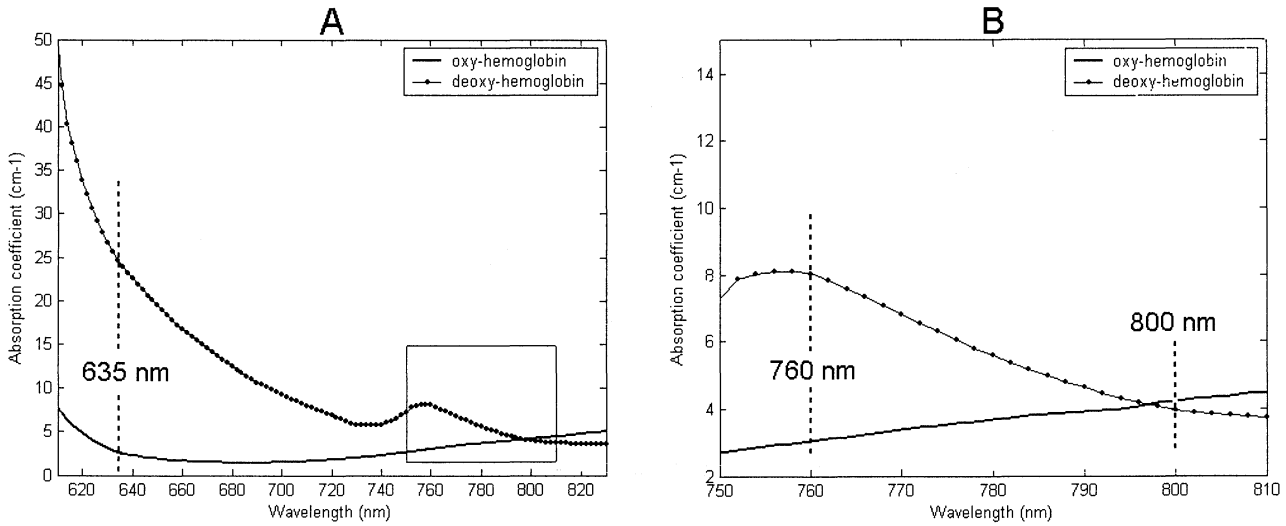

Figure 4.7. Absorption spectrum for deoxy-haemoglobin (Hb) and oxy-haemoglobin (HbO_2).In figure A you can see that deoxy-haemoglobin is a much stronger absorber than oxy-haemoglobin for wavelengths below 800 nm. The two molecules absorb equally much at 800 nm a fact which is used when measuring the oxygen saturation in blood, see figure B [18].

By using the measured fluence rate intensities and the solution to the time-independent diffusion equation, see chapter 3.5, the effective absorption coefficient at 760 and 800 nm can be calculated. If you assume that haemoglobin is the main absorber in tissue you can express the absorption coefficient as:

$$\mu_a^{760\,nm} \propto \varepsilon_{Hb}^{760\,nm}[Hb] + \varepsilon_{HbO_2}^{760\,nm}[HbO_2]$$
$$\mu_a^{800\,nm} \propto \varepsilon_{Hb}^{800\,nm}[Hb] + \varepsilon_{HbO_2}^{800\,nm}[HbO_2]$$

where ϵ denotes the extinction coefficient for the specific wavelength and compound. Using the fact that oxy- and deoxy-haemoglobin have the same extinction coefficients and the simplification, based on the assumption that $\mu_a << \mu_s'$ and that μ_s' is approximately constant over the wavelength range 760-800 nm:

$$\left(\frac{\mu_{eff}^{760\,nm}}{\mu_{eff}^{800\,nm}}\right)^2 = \frac{\mu_a^{760\,nm}(\mu_a^{760\,nm} + \mu'^{760\,nm}_s)}{\mu_a^{800\,nm}(\mu_a^{800\,nm} + \mu'^{800\,nm}_s)} \approx \frac{\mu_a^{760\,nm}}{\mu_a^{800\,nm}}$$

the formula for oxygen saturation can be rewritten as:

$$S_{O_2} = \frac{1}{\varepsilon_{Hb}^{760\,nm} - \varepsilon_{HbO_2}^{760\,nm}}\left(\varepsilon_{Hb}^{760\,nm} - \varepsilon_b^{800\,nm}\frac{\mu_a^{760\,nm}}{\mu_a^{800\,nm}}\right)$$

The absorption coefficients are known from the fluence rate measurements and the extinction coefficients are tabulated (Figure 4.7) so the oxygen saturation level can at last be calculated. Studies show that the oxy-haemoglobin concentration during treatment only declines at distances shorter than 3 mm from the fibre tips [19].

5 Optimization algorithms

Our main task in this master thesis project was to develop an algorithm that calculates the optimal placements of an arbitrary number of optical fibres (from the beginning 6 fibres) in an arbitrarily shaped tumour, prior to an IPDT-treatment. Optimal in this case are the positions generating the shortest possible treatment time and the least possible harm to sensitive surrounding tissue.

The idea is that these optimization calculations should be performed, based on a recently acquired 3D image (from e.g. ultrasound or MR), within a couple of minutes just prior to the treatment. This leads to certain speed requirements for the algorithm. We therefore decided that the total calculation time for the algorithm should be no longer than a couple of minutes.

To solve the task we have made certain simplifications, e.g. we assume the fibre tips to be isotropic light sources and we assume that the light fluence rate at any distance from a fibre tip can be described by Eq. 3.1 according to the previously described diffusion theory.

A further simplification is that we decided to work on a discretized geometry. Since the precision of the fibre placement will probably not be better than in the range of ±1-2 mm we decided that a discretization into mm-voxels would be suitable. We have thus mainly worked with geometries in the form of a discretized 3D-cube, wherein certain voxels represent the tumour and certain others represent especially sensitive tissue or other healthy tissue.

5.1 Main features of an optimization algorithm

In an optimization process there are always certain goals you want to achieve or certain parameters you want to optimize. This is usually expressed in the form of an objective function (fitness function) for which the resulting value should be maximized or minimized, depending on the formulation of the problem. In simple optimization problems there is only one object to fulfil, e.g. to find the shortest way between a certain number of points. This is called single-objective optimization. In cases like ours when you have two or more objectives; we want to minimize the treatment time and at the same time we also want to minimize the damage caused to surrounding healthy tissue, it is called multi objective optimization. This is a more complicated form of optimization since it requires that certain weights have to be given to the different objectives.

In our IPDT-application the two objectives were to minimize the treatment time, which is the same thing as maximizing the lowest fluence rate in the tumour, and to minimize damage to sensitive tissue, which means to minimize the highest fluence rates in sensitive tissue-areas.

5.2 Considered algorithms

Our search for the perfect algorithm for our very special application can be divided into two main parts. The first was a literature study of optimization algorithms for similar applications, such as brachytherapy and cryosurgery. The second part has been our own tests and implementations of different ideas for the algorithm for our IPDT-application.

Numerous articles treating the quite similar optimization problem for brachytherapy, was found. There are, though, some important differences between the brachytherapy optimization and our application. In brachytherapy a great number (~100) [20] of radioactive seeds are inserted in the tumour in parallel lines along the needles used for the implantation. In our case we have a low number of fibres (originally 6) that could be placed independently of each other. The brachytherapy optimization problem is thus different and maybe a little more complex than ours and the algorithms used for that application are often either very complex or only working on simplified geometries, such as a 2D-plane. Hence we decided to develop our own algorithms for our application using the ideas found in different articles [21-24]. Some of the tested algorithms are listed below. Most successful were the stochastic and genetic algorithms, which are described in detail.

5.2.1 Systematic algorithms

A first naive thought was to search through the whole geometry and try all possible combinations of voxels for the placement of the six fibres. This is the first solution method you have in mind and the most basic way of finding the best fibre position. To be able to evaluate a fibre position you must calculate how each fibre contributes to the total fluence rate distribution in all parts of the tumour. In more detail you must for each placed fibre add its fluence rate contribution to each tumour voxel. On how big tumours can you apply this method of going through all possible fibre positions without exceeding the time limit? Evaluating a fibre placement thus requires a lot of summations (see the calculation example below).

$$NoF = Number\ of\ Fibers$$
$$NoTV = Number\ of\ Tumour\ Voxels$$

$$NoF \cdot NoTV = number\ of\ summations\ for\ one\ fiber\ placement$$

Assuming a modern PC can perform around 10^9 summations each second you will be able to make $120 \cdot 10^9$ summations within the 2 minute time limit for our algorithm. One fibre position requires at least $NoF \cdot NoTV$ summations leading to maximum number of fibre placements of:

$$\frac{120 \cdot 10^9}{NoF \cdot NoTV}$$

When placing NoF fibres in a tumour of size $NoTV$ you can do it in $\binom{NoTV}{NoF}$ different ways.

Combining the two expressions from the last two paragraphs you get:

$$\binom{NoTV}{NoF} \approx \frac{NoTV^{NoF}}{NoF!} = \frac{120 \cdot 10^9}{NoF \cdot NoTV} \quad \text{assuming } NoTV >> NoF$$

Solving for $NoTV$ one obtains:

$$NoTV = \sqrt[(NoF+1)]{120 \cdot 10^9 \cdot (NoF-1)!}$$

If the treatment is performed using 6 optical fibres the maximum number of tumour voxels becomes:

$$\begin{aligned} NoTV &= \sqrt[(6+1)]{120 \cdot 10^9 \cdot (6-1)!} \\ &= \sqrt[7]{120 \cdot 10^9 \cdot 5!} \\ &= 75.8169 \approx 75 \; voxels \end{aligned}$$

If you only have 75 voxels at your disposal when representing e.g. a 40·40·40 mm big tumour you will end up with a resolution of:

$$\sqrt[3]{\frac{40 \cdot 40 \cdot 40}{75}} = 9.485 \; mm \; between \; each \; voxel$$

If you want a resolution of 1 mm trying out all possible fibre placements in the 40·40·40 mm tumour it would take:

$$T = \frac{NoTV^{NoF+1}}{(NoF-1)! \cdot 10^9} = \begin{bmatrix} NoF = 6 \\ NoTV = 40^3 \end{bmatrix} = \frac{40^{3(6+1)}}{5 \cdot 4 \cdot 3 \cdot 2 \cdot 1 \cdot 10^9} = 3.665 \cdot 10^{22} \; s \approx 10^{15} \; years$$

When treating such big tumours you have to use more fibres to avoid treatment times of several hours. If you use 18 fibres instead of 6 the computation time will be $5.839 \cdot 10^{63}$ s (using the same equation as above with NoF=18).

It's not hard to realize that it is impossible to use the 'try out all possible fibre positions'-method on a tumour of arbitrary size, using any number of fibres and at the same time keeping an acceptable resolution. The method was dismissed after the above considerations and thus never implemented.

Another idea of a systematic algorithm we actually tried out was an algorithm that for one fibre at a time tested a move of length 1 in all directions. This process turned out to give fairly good results but it was rather slow and could sometimes cause the fibres to get stuck in less favourable positions, i.e. the algorithm was not very robust.

5.2.2 Adjoint functions

The idea behind this optimization method is based on evaluating each possible fibre position based on its physical significance, which depends on factors like the tumour shape and the geometries of sensitive tissues surrounding it. An evaluation like this gives a priori information on how good it is to place a fibre at a certain position. The results from this evaluation can be used as guidance during the rest of the optimization process. When treating a tumour you want to deliver as high light dose as possible to the target region while sparing sensitive tissues, e.g. mucous membranes, blood vessels and in the case of prostate treatments the urethra and rectum. Each of these tissues is called a region of interest (ROI).

If you let Di,j denote the fluence rate in voxel i when a fibre is placed at position j the adjoint function for the voxel j for one ROI, e.g. the tumour, is defined as:

$$D_j^{Tumour} = \frac{\sum_i^N D_{i,j}}{N}$$

where N denotes the number of voxels in the ROI.

Unfortunately when treating tumours you will notice that it often is impossible to treat 100 % of the target area while sparing 100 % of the sensitive tissues from a too high dose. The interests are most of the time contradictory; this is what multi-objective optimization is all about. You have to find a way to balance your interests and one way of doing this is to use a quotient were all interests are included. In our case an 'adjoint quotient' is made:

$$R(j) = \frac{\sum_{k=1}^{all\ sensitive\ ROI} w_k D_j^k}{D_j^{Tumour}}$$

where w_k is a weight factor specific for sensitive tissue k. A good fibre position has a low 'adjoint quotient' while a not so good solution has a higher quotient. After calculating a quotient for every possible fibre position j a plot of the 'adjoint quotient' as a function of fibre position can be made. In Figure 5.1A an example of adjoint functions and adjoint quotient for a 2D-image of a prostate can be seen. Figure 5.1B shows a 3D-plot of how the adjoint quotient varies with the possible fibre position in the 2D-image.

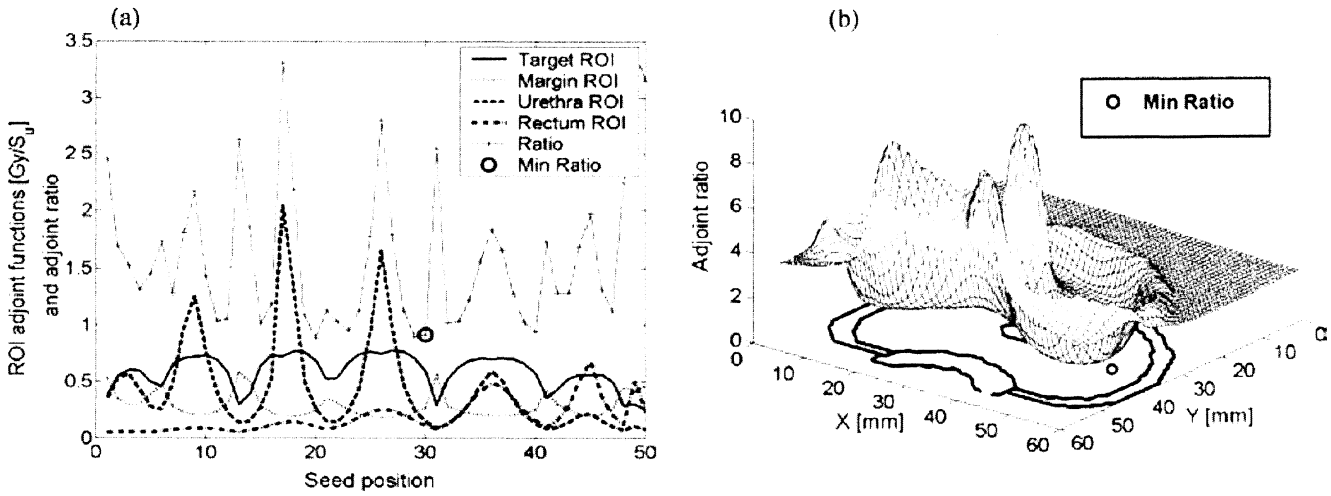

Figure 5.1 (A) the adjoint quotient calculated from the ROI adjoint functions. Both the adjoint quotient and functions are plotted. The minimum point is marked by a circle. (B) shows how the adjoint quotient changes with the possible fibre positions in the 2D-image. The two images are from [23], describing seed positioning in brachytherapy. This explains why the ROI adjoint functions are given in Gy/source unit and why the x-axis in (A) have the unit seed position instead of fibre position.

The evaluation of the possible fibre positions is now finished and the adjoint quotients can be used as guidance for positioning the fibres. One way of doing this is to use a so called greedy algorithm that places the fibres one at a time without revising earlier decisions when placing the following fibres. This can e.g. be done by placing the first fibre at the position having the global minimum value among the adjoint quotients. To avoid placing fibres too close to each other, the fibres are not allowed to be placed within a certain radius from the each other. The second fibre is placed in the position having the global minimum in the now reduced set of adjoint quotients. When placing the third fibre even more possible fibre positions are excluded and the set of adjoint quotients is reduced even further. The rest of the fibres are placed following the same procedure.

As mentioned earlier the main difference between positioning optical fibres in IPDT and radioactive seeds in brachytherapy is the number of sources to be positioned. When treating e.g. a prostate with brachytherapy around 100 seeds are used [20], whereas IPDT-treatment requires the use of 10-20 optical fibres to achieve a reasonably short treatment time. In brachytherapy you have enough sources to simplify the optimization process by slicing 3D-image into several 2D-images and performing the optimization of seed positions in each 2D-image independently of each other. In IPDT you have much less sources and are forced to perform the optimization in 3D.

When implementing the adjoint quotient solution method to our IPDT problem we expanded the adjoint quotient calculation from 2D to 3D. When extending the method to 3D you unfortunately loose the 2D methods best quality, its rapidity.

The main reason for not pursuing with the adjoint quotient method was not the computation time but the lack of local minima in the 3D-matrix of adjoint quotients. When going from 2D to 3D many of the local minima in a cross section of the 3D-image

appears to flood into each other in a nearby 2D-slice and thereby diminish the number of local minima in the 3D-matrix of adjoint quotients.

Even though we calculated adjoint quotients for several oddly shaped tumours with many surrounding sensitive tissues we never got more than 5 local minima points in the 3D-matrix of adjoint quotients. The adjoint quotient method was abandoned because it was too slow to be a good method for generating start coordinates and too inaccurate to be used alone.

5.2.3 Deterministic algorithms

One early idea was to try the algorithm used by Olsson and Rylow [25] in 1998 treating the same problem of fibre placement optimization. The idea of their algorithm was to identify the point in the tumour where the fluence rate was lowest and then move one of the fibres closer to that point. Then this procedure should be repeated until no further improvement could be achieved. This type of algorithm can be seen as a deterministic search through the geometry from a given start position. It is deterministic since the final result theoretically can be calculated in advance i.e. one given start position will always generate the same solution. The objective function (F) to maximize that was used here can be written as follows:

$$F = \min\{\varphi \in tumour\}$$

Spontaneously this deterministic search process sounded like a good idea but our tests of this algorithm showed that there was a great tendency for the fibres to get stuck in really bad positions using this algorithm. Often two or more fibres ended up in a cluster which is a clearly unfavourable solution since we want an even light distribution in the tumour.

One of the reasons why this algorithm failed is quite easy to understand. Imagine that the fiber positions reach a stage where the same lowest fluence rate in the tumour can be found in two points situated in opposing parts of the tumour. Any move towards one of these points will in that case automatically lead to a decrease in the fluence rate for the other of the two points and the algorithm will terminate its search for better positions.

One possible improvement of the previous algorithm was to expand the objective function. Instead of only considering the one point with the lowest fluence rate in the tumour we now took into accounts many more e.g. the 500 voxels receiving the lowest light dose (fluence rate). The new objective function could be expressed as:

$$F = \sum_{500\ lowest} \{\varphi \in tumour\}$$

This modified version of the first algorithm, still based on moving the fibres towards the point with the lowest fluence rate, turned out to be quite fast and to give quite good solutions if given acceptable start positions, i.e. quite well-distributed fibres in the

geometry. Some drawbacks, e.g. some instability in the form of a slight cluster-tendency, could though still be found and we decided to move on to other types of algorithms. At this stage we also introduced sensitive tissue areas in the geometry. This made us modify the objective function to also include a negative term for the highest fluence rate in the sensitive areas:

$$F = \sum_{500\ lowest}\{\varphi \in tumour\} \quad - \sum_{150\ highest}\{\varphi \in sensitive\ tissue\}$$

One solution that seemed fairly good for the used objective function, given by this algorithm for a 2D-geometry, can be seen in Figure 5.2. The number of voxels of each tissue type used in the above stated objective function is just an example; we have tested many different combinations of numbers. The basic idea of this objective function, summing fluence rates from tumour voxels and subtracting fluence rates from sensitive voxels, is what we used in our further work.

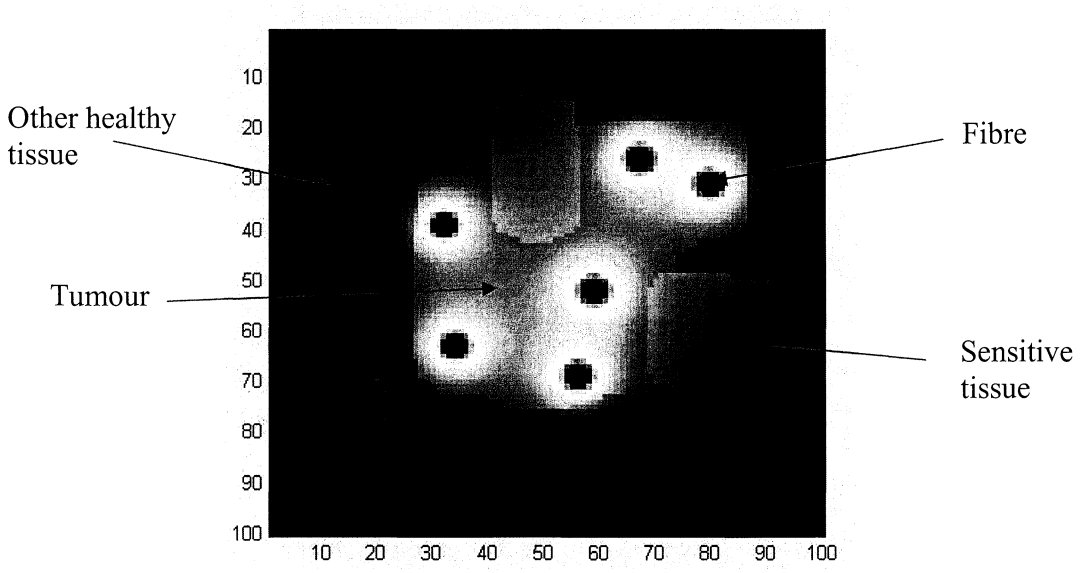

Figure 5.2 Solution provided for a simple 2D-geometry by one of the first deterministic algorithms. The fluence rate is plotted in the entire geometry to give an idea of the dose the sensitive areas would receive. To visualize the borders between different tissue types a constant is added to the fluence rates in the sensitive tissue whereas a constant is subtracted from the fluence rates for other less important healthy tissue.

Another idea of a deterministic algorithm we tried out was a function identifying all local fluence rate minimas in the tumour and then moving each fibre closer to the closest local minima. This algorithm was fast and could sometimes improve the result from the previous algorithms, but a great tendency for the fibres to end up in clusters could still be observed. This can easily be explained by the fact that in the middle of three close-lying fibres there can always be found a local fluence rate minima.

The recurrent problem for the deterministic algorithms is the tendency of clustering and that the fibres too often get stuck in unfavourable positions. To avoid this problem we tried some stochastic algorithms.

5.2.4 Stochastic algorithms

Our first idea of a stochastic algorithm was a function generating totally random fibre configurations within the tumour. Repeating this procedure a large number of times and then selecting the best proposition (the one generating the highest fitness value) would maybe give some acceptable results. Our tests have shown, though, that this hardly ever generates any good results in a reasonable time even for very small geometries and only 6 fibres. This algorithm we further on refer to as the 'Random Search'-function.

Another idea of a stochastic algorithm was a function that from a given a start position iteratively move the fibres stochastically around in the tumour in the search for better configurations. In this way the algorithm could quite effectively search through the space of possible solutions without getting stuck too easily in local minima. To make this algorithm a little more intelligent the stochastic moves were limited in length. The length of the moves is also decreased with time to facilitate the fine adjustment when approaching the optimal solution. Any move resulting in a lower fitness value is cancelled. This algorithm turned out to be medium fast and relatively stable, quite often resulting in solutions that seemed to be optimal for the given object function. Further on, we refer to this algorithm as the 'Random Move'-function.

5.2.5 A genetic algorithm

Genetic programming is a search method for solving optimization problems. It was originally developed by John Holland et al. at the University of Michigan in the beginning of the 1970's [26]. The idea behind the method is to mimic nature's mechanism of natural selection and adaptability. An evolution is simulated using artificial creatures, in our case possible solutions to our optimization problem. Each creature's reproduction capability depends on its ability to adapt to some stated criteria (objective function). In every new computation round, a so called generation, a new set of creatures are created by random crossing and mutation of creatures. The mutation makes sure that new parts of the search space are explored. Each new creature is then evaluated using an objective function and is thereby given a fitness value that determines its probability to survive and become a part of the next generation.

Based on the fact that our problem is a geometrical problem we have created two geometrical operations that a solution can be exposed to. The two operations are rotation and translation of the coordinates. We used a so called elitist algorithm to constantly guarantee the survival of the best individual (solution) when the population is reproduced. The best individual automatically moves on to the next population without experiencing the reproduction process. In our genetic algorithm the best solution is also

spared from the genetic and geometric operations i.e. crossing, mutation, rotation and translation.

In Figure 5.3 a flow scheme of our genetic algorithm can be seen. The program starts by creating a start population consisting of randomly drawn numbers as start coordinates. The population is reproduced i.e. each individual is evaluated using an objective function which also determines the probability for the individual to survive and thereby be a parent to the next generation. You can see all the individuals' probability to survive as a roulette wheel and each individual's probability as a part of that wheel. By turning the wheel you can randomly pick out one individual that will survive the reproduction. A high fitness value gives a high survival probability.

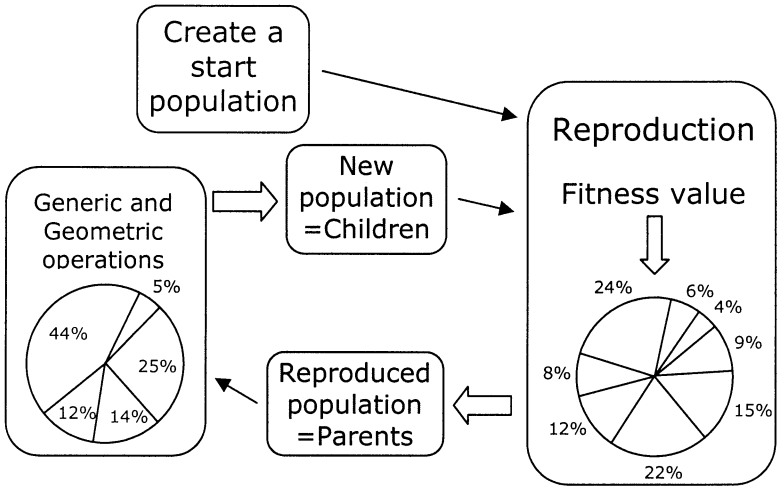

Figure 5.3 A schematic picture of how our genetic algorithm works. First a start population is randomly created and reproduced. After reproduction all individuals in the population might be exposed to one of the following operations: rotation, translation, crossing or mutation according to specified probabilities. In this way a new population is created and ready for evaluation and a new reproduction.

The individuals that get through the reproduction can be seen as parents to the next generation's individuals. The next generation is created by rotating, translating or mutating individuals or by the crossing of two individuals. An individual can only be exposed to one of these four operations and there is also a chance that it will go through unchanged. The probability for performing a certain operation on an individual depends on which operation it is. Some operations are more probable to occur than others. During the part of genetic and geometric operations each individual experiences a second roulette selection process having five possible outcomes, the four operations and the alternative of getting through unaltered.

After the genetic and geometric operations a new population has been created, often called the children. One computation round in the genetic algorithm is now finished and when the new population enters the reproduction part a new round is started. The switching between reproductions and performing operations on the population continues while there's computation time left.

5.3 The final algorithm

The main drawback of the genetic algorithm is that it is rather time-consuming in our application.

The algorithm which has shown the best performance results is a development of the 'Random Move' algorithm mentioned above wherein the 'Random Move' procedure is repeated several times for different startpositions generated by the 'Random Search' algorithm. The number of restarts with new random startpositions for a given runtime is dependent on the size (number of voxels) of the tumour. A small tumour implies fewer calculations and thus the algorithm has time for more restarts. This final algorithm, which can be seen as stochastic but intelligent, has proved to be very stable, almost always resulting in very good solutions. In addition it is much faster than the genetic algorithm. The solution for one of the first 3D tumour geometries we tried ("tumour 1", see Appendix) can be seen in Figure 5.4 below.

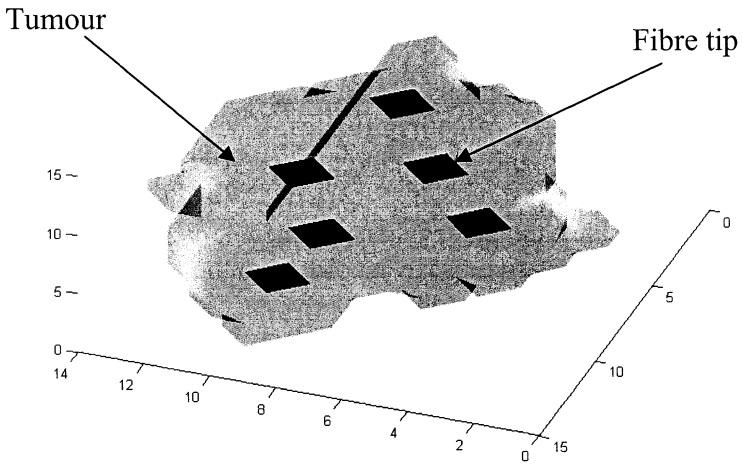

Figure 5.4 Solution provided by the 'Random Move'-algorithm for a small 3D tumour geometry. The suggested fibre tip positions are represented by the dark dots in the geometry.

6 Implementation

6.1 Main data structures

During the optimization procedure four main data structures are used to represent the tumour geometry and to calculate each solution's fitness value. The structures are:

- Tissue Matrix
- Flow Matrix
- Tumour Matrix
- Sensitive Tissue Matrix

More detailed information about how both 'Random Move' and the genetic algorithm is implemented and "User guidelines" can be found either at SpectraCure AB, Sweden, or at the Atomic Physics Department at LTH, Sweden.

6.1.1 Tissue Matrix

The Tissue Matrix is a 3D-matrix based on a medical image of the tumour taken using either an ultrasound or a MRI apparatus. It can be seen as a discrete or a low resolution 3D-image of the tumour and its surrounding tissues. It contains all necessary geometrical information about the tumour, the surrounding tissue and any sensitive tissues. Each matrix element also constitutes a weight factor used in the optimization of the fibre positions. Depending on an element's value it either constitutes a part of the tumour, normal insensitive tissue or sensitive tissue according to the following listing:

> 0, *Tumour tissue*
$= 0$, *Normal insensitive tissue*
< 0, *Sensitive tissue*

The element's value can thus both be used for discrimination and weighting. A voxel with value -2 is therefore a part of a sensitive tissue and has the weight factor 2. The voxel weight factor is proportional to the voxels importance in the fitness calculation. A voxel weight factor of 1 influences the solution's fitness value only half as much as a voxel with the value 2.

6.1.2 Flow Matrix

In order to evaluate a fibre position you have to calculate the fluence rate, caused by its specific fibre coordinates, in all parts of the tumour and sensitive tissues. To minimize the computations we chose to calculate all possible fluence rates once and storing those in a 3D-matrix called Flow Matrix. The source is placed in the middle of the Flow Matrix which has twice the dimensions of the Tissue Matrix. Using the solution to the time-

independent diffusion equation (Eq. 3.1) and all necessary input values (e.g. fibre power and optical properties) the fluence rate in all parts of the matrix can be calculated.

6.1.3 Tumour Matrix

The Tumour Matrix is a numerical 2D-matrix containing the x-, y- and z-coordinates of all tumour voxels together with its weight factor. It has the dimension 'number of tumour voxels'·4. Each row in the matrix contains all information about one of the tumour voxels. The first three elements contain the x-, y- and z-coordinates and the fourth element contains the weight factor.

6.1.4 Sensitive Tissue Matrix

In this vector all the coordinates and the sensitive tissue voxels weight factors are stored in the same way as in the Tumour Matrix above.

6.2 Objective function

The objective function is calculated by first adding the fluence rates from a given percentage of the tumour voxels having the lowest fluence rate. The same procedure is performed on the sensitive tissue voxels having the highest fluence rate but not necessarily using the same percentage. Finally the two contributions are added together. Thus the objective function can be expressed as:

$$F = \sum_{i=1}^{M} w_i \phi_i + \sum_{j=1}^{N} \omega_j \phi_j \qquad \text{(Eq. 6.1)}$$

ϕ_i = *fluence in the tumour voxel having the* i *: th lowest fluence*

ϕ_j = *fluence in the sensitive tissue voxel having the* j *: th highest fluence*

w_x = *weighting factor for voxel* x

M = *number of tumour voxels to be included*

N = *number of sensitive tissue voxels to be included*

where N and M are given by multiplying the number of tumour and sensitive tissue voxels respectively with a given percentage.

Since the fluence rate in each voxel is multiplied by its weight factor before the summation is made the 'tumour voxel sum' will be positive while the 'sensitive tissue voxel sum' will be negative. A good fibre placement therefore has a high fitness value.

6.3 Calculation Procedure

A possible solution is evaluated by calculating its fitness value according to the Objective function (see chapter 6.2). This is done by first calculating the fluence rate in each tumour and sensitive tissue voxel for the specific set of fibre coordinates. In more detail the total fluence rate in a voxel is calculated by adding the fluence rate contributions from all fibres together. By calculating the difference in coordinates between a voxel and a fibre, the fluence rate contribution from that fibre to the voxel can be calculated using the Flow Matrix that contains all possible values of fluence rate contributions.

The fluence rate in each tumour voxel is then multiplied by the voxel's specific weight factor and consecutively inserted into an array of length 'number of tumour voxels'. All sensitive tissue voxels are treated in the same way with the exception of being placed in an array of length 'number of sensitive tissue voxels'. After all fluence rates are inserted into the two arrays they are sorted in ascending order.

Finally the solutions fitness value is calculated using the two sorted fluence rate arrays and in accordance with the Objective function.

7 Optimization tests and results

To verify that the developed algorithm works as it is supposed to, different tests have been performed and the results have been plotted in various sorts of diagrams. Five different tumour geometries were created for the tests; two randomly shaped ("tumour 1" and "tumour 2"), one prostate like, one sphere and one cube. See appendix for pictures of the different geometries.

7.1 Manual placement

To show that there really is a need for a good optimization algorithm we gave our colleagues in the Medicine group at the Atomic Physics Department, the possibility to try to manually place 6 fibres in the 3D prostate geometry. A small test procedure in Matlab was developed for this purpose. The program allowed the test person to rotate the geometry and view it from all possible angles. The fibre configuration could be changed and reviewed until a satisfactory result was obtained. The proposed fibre coordinates were then tested by one objective function to find out their fitness values. Finally we let the algorithm propose fibre configurations using the same objective function. See Table 7.1 and Figures 7.1 and 7.2 below. For further comparison we checked the mean fitness value for 12 randomly obtained configurations. As can be seen in Table 1, the algorithm gave markedly better solutions as indicated by the higher fitness value.

Results:

Creator of fibre configuration	Fitness value
Colleague A	0.0035
Colleague B	-0.0338
Colleague C	-0.0852
Colleague D (best)	**0.0127**
Colleague E	-0.0329
Colleague F	-0.0459
Random (mean value)	-0.0845
The algorithm	**0.0387**

Table 7.1 Fitness values for the fibre configurations proposed by some of our colleagues. To be compared with the mean value of random configurations and the fitness value for the configuration provided by our algorithm.

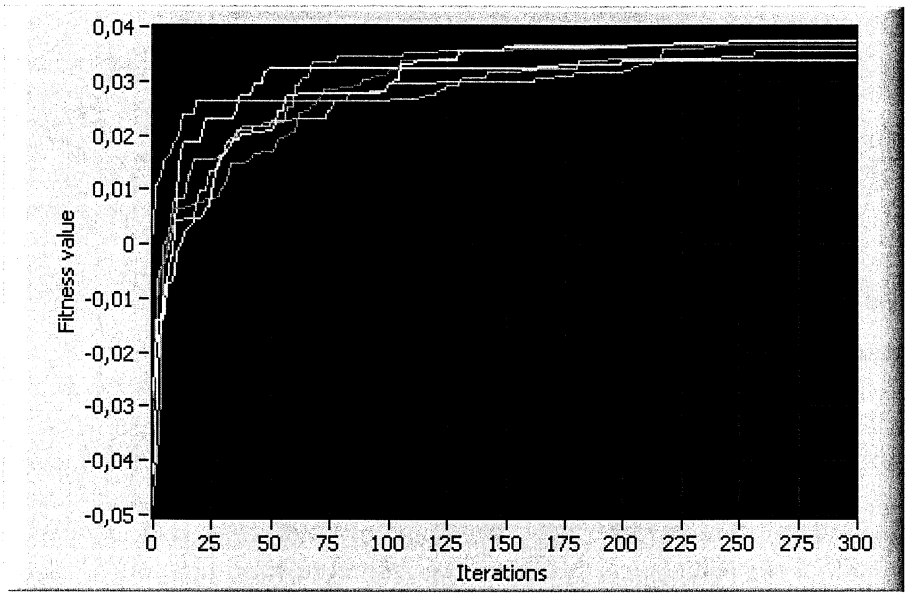

Figure 7.1 The fitness value development in the algorithm from six different random start positions, using the fitness function from the manual placement tests. It can be noted that the fitness value 0.0127 (best result from manual test) is passed already after 10-30 iterations.

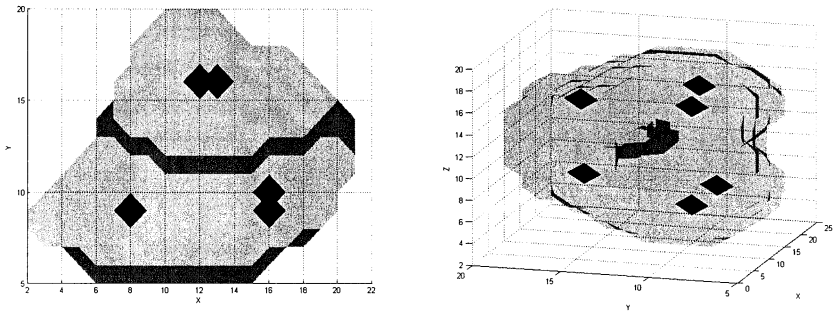

Figure 7.2 The prostate geometry with the fibre coordinates proposed by the algorithm.

7.2 The sphere

For a sphere-geometry it is possible to analytically calculate the optimal positions for 6 fibres. To verify that our algorithm works, we therefore decided to create a sphere-shaped tumour and try the algorithm on this geometry.

It is easily realized that the optimal positions for six fibres in a sphere is one fibre on each of the six coordinate axes in a system with origo in the centre of the sphere (see Figure 7.3 A). The question is then how far from the centre of the sphere the fibres should be placed to maximize the lowest fluence rate.

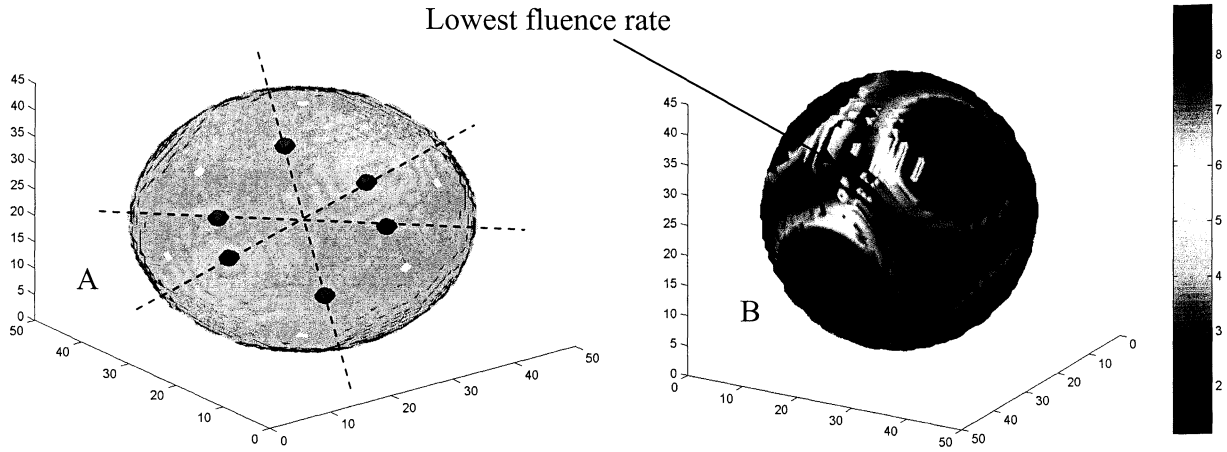

Figure7.3 A) Optimal positions for a sphere-geometry. B) The fluence rate at the surface of the sphere.

It is obvious that the lowest fluence rate can be found in the point $\left(\frac{1}{\sqrt{3}},\frac{1}{\sqrt{3}},\frac{1}{\sqrt{3}}\right)$ if the fibres are placed on the axes in a sphere of radius = 1. (See Figure 7.3 B and the corresponding case for a 2D-geometry in Figure 7.4). It is thus the fluence rate in this point, point A in Figure 7.4, (and the other 7 corresponding points) that should be maximized. Spontaneously you then think that the optimal positions for the fibres are $1/\sqrt{3} \approx 0.577$ ($1/\sqrt{2}$ for the 2D-case) out from the centre to put the fibres as close as possible to these points.

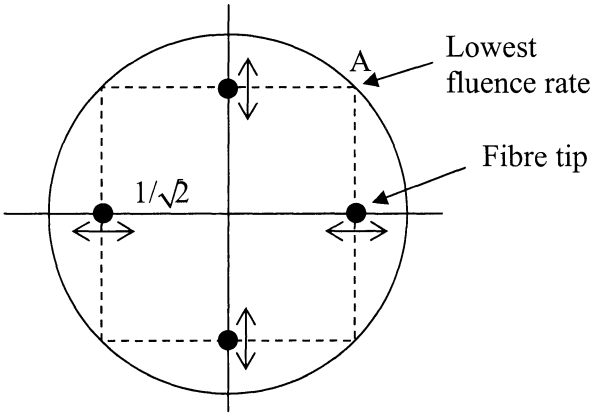

Figure 7.4 The same problem for a 2D-geometry.

A calculation we performed in Matlab (for certain given optical properties) did show, though, that the optimal positions were situated approximately 0.52 out from the centre if only the one voxel with the lowest fluence rate were considered in the optimization (see Figure 7.5). This can probably be explained by the contribution to the fluence rate from

the fibres on the opposite side of the sphere. Simultaneously decreasing the distance to the centre for all fibres starting from the 0,577-positions probably causes a larger increase in fluence rate contribution, in point A, from the three distant fibres than the decrease in contribution from the close-lying fibres. This since the distances to the three distant fibres decreases more than the distance to the close-lying fibres increase.

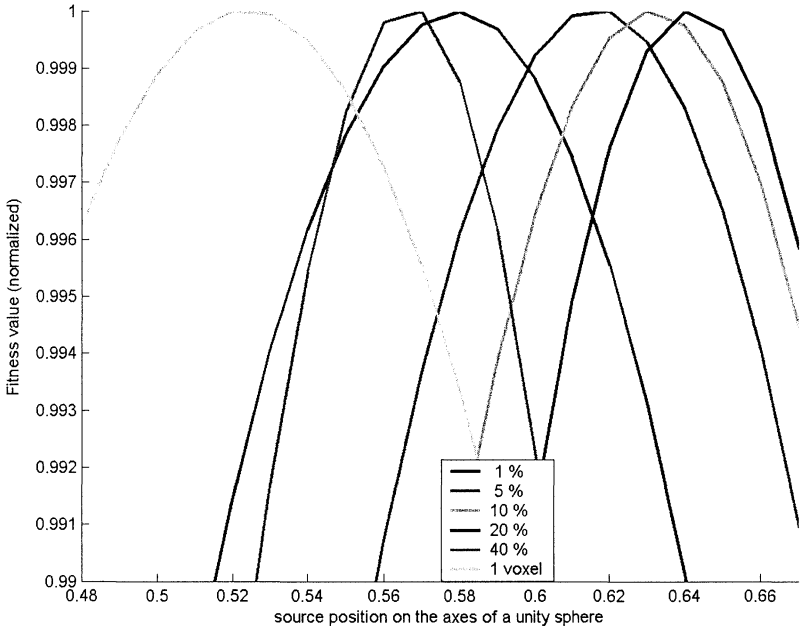

Figure 7.5 Diagram showing the optimal source positions on the axes in a unity sphere, when including different percentages of the tumour voxels in the fitness function.

Anyway, the result of this test was that our algorithm in fact did propose fibre configurations that corresponded well with the theoretically optimal positions. Depending on the number of voxels included in the fitness function the algorithm proposed a distance of between 0.5 and 0.6 out from the centre of the sphere.

7.3 Fluence rate histograms

In order to illustrate the proposed solution we also integrated the possibility to plot fluence rate histograms for the calculated fibre configuration in a given geometry. Histograms for the fluence rate in both tumour and sensitive tissue are given in the LabView-version in the developed program. Two results for the prostate geometry are shown in Figure 7.6 A and B below. The same fitness function is used but in the A-figure the algorithm has proposed a configuration for 18 fibres whereas in the B-figure only 6 fibres are used. As can be seen sensitive tissue is spared from too high light doses.

A

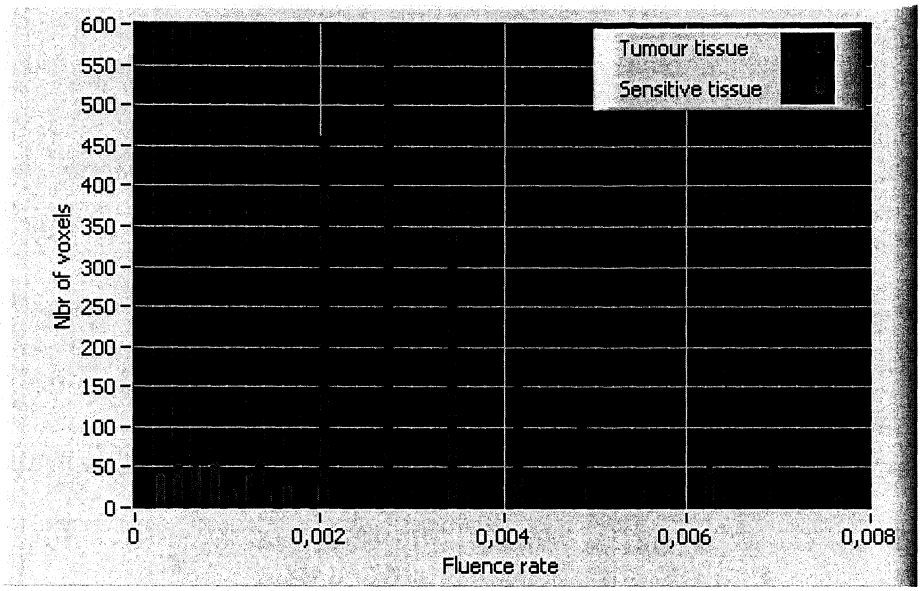

B

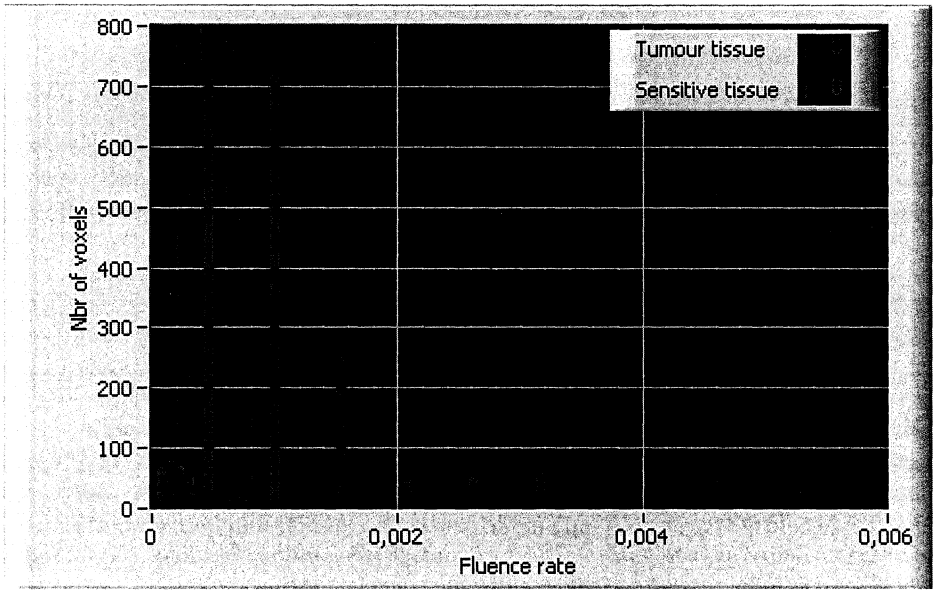

Figure 7.6 Histograms showing the number of voxels in each fluence rate-interval, for "optimal" fibre configurations in the prostate geometry. Fluence rate is here given in W/mm2. In figure A, 18 fibre positions are optimized whereas in figure B only 6 fibres are used.

7.4 Performance statistics

To try out the performance of the algorithm we carried out a great number of repeated tests on the different tumour geometries and the resulting fitness values were compared. The result of this performance test is shown in Table 7.2. Three different tumour geometries, with 547, 1874 and 5324 voxels, have been used. The rightmost column

displays the result as the percentage of the total number of runs that resulted in the maximum fitness value for the objective function used.

One should note that even though a certain test run did not result in the optimal fibre positions, the proposed solution often gave a fitness value close to the maximal value. This is also illustrated by the fifth and sixth columns, listing the minimal and maximal fitness values of the resulting solutions.

Test	Tumour size (voxels)	Time /run	Restarts /run	Max fitness	Min fitness	Mean fitness	% max
30 runs on tumour 1	547	110 s	10	9.25927	9.20998	9.25411	83 %
200 runs on tumour 1	547	10 min	51	0.19451	0.19451	0.19451	100 %
100 runs on prostate geometry	1874	6 min	10	18.0693	17.9693	18.057	82 %
50 runs on prostate geometry	1874	10 min	15	0.169128	0.168525	0.169116	98 %
50 runs on prostate geometry	1874	10 min	15	0.0495831	0.0489361	0.0495721	98 %
200 runs on tumour 2	5324	12 min	3	0.240475	0.236748	0.240291	51 % (90 %)

Table 7.2 Results of algorithm tests. The last column indicates the percentage of the runs that resulted in the maximum fitness value (the optimal solution) for the chosen objective function. The value in parenthesis indicates the percentage of the runs resulting in the best or second best solution. Restarts/run indicates the number of times the algorithm had time to restart with a new random start position. The varying size of the fitness values are due to the used fitness functions. The computer used for the tests was an Intel Celeron CPU 1300 MHz, 248Mb RAM.

7.5 Comparison with the genetic algorithm

To further evaluate the performance of the algorithm we compared it to the genetic algorithm that we also developed and implemented ourselves. We let the two algorithms perform 50 test-runs of 6 minutes each on the prostate geometry. For comparison the fitness values obtained in the manual test (see section 7.1) and the fitness values from the 12 random configurations were included in the table:

Algorithm	Highest fitness value	Lowest fitness value	Mean fitness value
Genetic	0.030721	0.022919	0.028417
'Random Move'-based	0.0387369	0.0360484	0.0375705
6 manually proposed	0.0127	-0.0852	-0.03026
12 random placements	-0.02774	-0.17869	-0.08448

Table 7.3 Results from the comparison with our genetic algorithm.

From Table 7.3 it is quite obvious that the 'Random Move' algorithm performed better that the genetic algorithm. The main advantage of this stochastic method was the ability to always give, if not optimal, close to optimal fibre positions. This is indicated by the minimal fitness value in the third column, which is markedly higher for the 'Random Move'-based algorithm.

8 Discussion and conclusions

Generally we have demonstrated a satisfactory behaviour and performance of the developed algorithm. It has proven to be relatively rapid, stable and gives results in agreement with the analytical solution for the spherical geometry. Each of the evaluation tests is commented on in the following paragraphs.

8.1 Manual Placement

The manual placement test clearly proved that there is a need for an optimization algorithm. Even though the best fibre configuration, proposed by colleague D, turned out to generate a fairly high fitness value, the algorithm could easily, and very fast, find even better solutions. See Figure 7.1.

The test also showed that it is difficult to manually place the fibres in tumour geometries even if you have the possibility to view the geometry from all possible angles. The configurations that some of the colleagues proposed (e.g. colleague E) looked quite good from two or three angles but viewed from yet another angle they were obviously far from optimal.

8.2 The sphere

The sphere-test showed that the algorithm proposes a solution that is optimal or close to optimal for a sphere-geometry, even though the exact positions depend on the number of voxels included in the objective function. Symmetrical geometries, such as the sphere, require a lower percentage of the tumour voxels included in the fitness function, than more oddly shaped geometries.

There is though a little risk that the 'Random Move'-algorithm gets stuck in non-optimal configurations for this completely symmetrical geometry. This minor problem is easily overcome by letting the algorithm restart a few times with new start coordinates, which is also automatically done in the final algorithm. Increasing the number of fibres also eliminates this problem. An important note is also that the problem of getting stuck in bad configurations never has been observed for the more realistic random-shaped tumour geometries.

Interesting were also the results showing how the optimal configuration varied with the different percentages of voxels included in the fitness function (see Figure 7.5).

8.3 Fluence rate histograms

A fluence rate histogram is a very good way to verify that a proposed solution for the fibre configuration generates a theoretically satisfying treatment effect.

The histogram in Figure 7.6A shows that this configuration (proposed by the algorithm) of 18 fibres in the prostate geometry, is a good solution. As can be seen, there are no really high fluence rates in the sensitive tissue voxels. At the same time most tumour tissue voxels receive a relatively high dose. A certain overlap of the fluence rates in the sensitive voxels and the tumour voxels is inevitable in a geometry like this with sensitive tissue (urethra) in the middle of the tumour.

The histogram in Figure 7.6B indicates that it is probably insufficient to use 6 fibres for a tumour geometry as complex as the prostate. Here, quite a large overlap of the fluence rates in the sensitive tissue voxels and the tumour voxels can be seen, which is clearly unfavourable. By using 18 fibres, a better selectivity can be achieved, as indicated in Figure 7.6A.

The exact appearance of a desired histogram would of course depend on the threshold for inducing necrosis in the malignant regions and the maximum allowed fluence rates in the sensitive tissue regions. These threshold values differ depending on the tissue type and the location in the human body, and their exact values are still unknown.

Worth to notice here is that the program does not take into account that the sensitive tissue probably has a different (usually lower) absorption coefficient. The absorbed dose in the sensitive tissue will therefore in reality probably be lower than what is demonstrated by the fluence rate histograms.

8.4 Performance statistics

The results from these repeated tests clearly show that our algorithm always can find the optimal solutions for the tested geometries. It is only a question of the time limit you give the algorithm and the size of the tumour. If the algorithm has time to restart with new random start positions more than approximately 15 times in a run it is almost certain that it will find the optimal solution. For the smallest tumour geometry tested ("tumour 1") with a size of 547 voxels a run with 15 restarts takes approximately 3 minutes. For the largest geometry ("tumour 2") with a size of 5371 voxels a run with 15 restarts takes approximately 30 minutes.

Important to note here is that almost all solutions that are "non-optimal" are still very good solutions. It is thus safe to run the algorithm a much shorter time.

8.5 Comparison with the genetic algorithm

This comparison showed that a pure genetic algorithm is slower and does not generate as good solutions as the stochastic 'Random Move'-based algorithm. This can be explained by the fact that the genetic algorithm is based on the evolution of a large population of e.g. 40 individual solutions. For each iteration this thus requires that the fitness value is

calculated 40 times. In comparison the 'Random Move'-algorithm works with one individual solution at a time which obviously is faster. To compensate for the lack of genetic diversity, the 'Random Move'-algorithm are given several different randomized start positions to work on.

Further, the genetic algorithm seems to have problems to reach the really optimal solutions for a given fitness function. This could probably be explained by the fact that a genetic algorithm continues to try large genetic changes, such as crossover and mutation, on the individuals even when they are close to the optimal solution. This makes the genetic algorithm very slow in the final converging towards the optimal solution.

The genetic algorithm might anyway be interesting for future development, though, since it theoretically is a very stable form of optimization algorithm. A modified genetic algorithm was used by Lahanas et al. for the brachytherapy optimization with a good result [22].

8.6 The objective function

Optimizing a process most often involves the task of minimizing an objective function. You can express the objective function in many different ways. The most important thing about the objective function is that it should reflect the optimization goals.

If your optimization goal e.g. is to maximize the fluence rate in tumour tissue while minimizing the fluence rate in sensitive tissues you should preferably have a function that punishes a too high fluence rate in sensitive tissues and rewards an even distribution of fibres. The following objective function, taken from the optimization for brachytherapy [21], fulfils the requirements of the above stated optimization goal:

$$F = \sum_{i=1}^{N}\left[w_i(\phi_{pre} - \phi_i)^2 + \alpha S_T(\phi_i - \phi_U)\right] + \sum_{j=1}^{M} w_j S_{ST}(\phi_j^{\max} - \phi_j)$$

N = *number of tumour voxels*

M = *number of sensitive tissue voxels*

w_i = *weighting factor for tumour voxel i*

w_j = *weighting factor for sensitiv tissue voxel j*

ϕ_{pre} = prescribed target *fluence in the tumour*

ϕ_x = *the acual fluence in voxel x*

ϕ_U = *upper fluence* limit *in the tumour*

$\phi_j^{\max}$ = *upper fluence* limit *in the sensitive tissue voxel j*

α = *penalty factor per fluence unit* (W/m^2)

$$S_T = \begin{cases} 0, (\phi_i - \phi_U) < 0 \\ 1, (\phi_i - \phi_U) > 0 \end{cases}$$

$$S_{ST} = \begin{cases} 0, (\phi_j^{\max} - \phi_j) > 0 \\ 1, (\phi_j^{\max} - \phi_j) < 0 \end{cases}$$

The strength of this objective function is that all voxels are included i.e. the fluence rate in each and every voxel is taken into account and that both too high and too low fluence rates are suppressed.

The big drawback when applied to IPDT dose optimization is that it contains threshold values. What threshold values you should use is dependent on the delivered dose. The major difference between a dose optimization in brachytherapy compared to IPDT is that the dose to be delivered from each seed in brachytherapy is known before the treatment and can be used during the optimization of the seed positions. In IPDT the delivered dose from each fibre is not known, before the treatment is performed, and the optimization of the fibre positions is made using only the information on the fluence rate distribution in the tissue, not the unknown delivered dose. Since the delivered dose is proportional to the absorption coefficient and, most important of all, to the treatment time, the delivered dose can never be exactly known before the light distribution has been modelled in detail.

One way of dealing with the problem is to estimate the treatment time, depending on the number of fibres used and the tumour size and shape. The treatment time will then determine the threshold values. Further complications are that the optical properties of each patient are not exactly known and that the treatment probably induces significant changes of the absorption coefficient [12]. Therefore the calculated treatment time will also probably be different from the actual treatment time, leading to inaccurate threshold values.

We circumvented the problem by simply choosing a different objective function, a function without threshold values (see chapter 6.3). The idea behind the function is to reward a high mean fluence rate in the e.g. 10 % of the tumour voxels with the lowest fluence rates while punishing for a high mean fluence rate in the e.g. 10 % sensitive tissue voxels with the highest fluence rates. The advantage of using an objective function like this is its simplicity and thereby rapidity. Not having to use threshold values can also be seen as a positive quality, since you don't have to rely on the accuracy in the estimations of the threshold values. The drawback of not using threshold values is that you lose the ability to use medical facts, e.g. the allowed dose in a certain sensitive tissue, in the optimization process.

It's hard to analyse and compare different objective functions in theory. The best thing is to test them on real tumour geometries and analyse the result in form of fluence rate histograms (see section 7.3).

Interesting to discuss is also how to choose the percentages in the objective function we have chosen to implement. This can also be empirically tried out by testing the algorithm

on various tumour geometries. Generally the tests we have performed show that lower percentages (~10%) for the tumour voxels are applicable on symmetric shapes such as the sphere or the cube, while it is better to use higher percentages (~20-30%) for more complex and/or randomly shaped geometries. How to choose the percentage for the sensitive tissue is really dependent on the size, shape and position of the sensitive tissue areas.

8.7 Other aspects

One question that has not yet been addressed is how to choose the number of fibres for a given tumour geometry. Generally a low number of fibres is to prefer for the convenience of the patient, since each inserted fibre involves a penetration of the tissue. A high number of fibres is to prefer if your only goal is to optimize the dose distribution in the tumour and to minimize the treatment time (see Figure 7.5). Our conclusion is that for small tumours of simple shape only a few fibres is the best solution whereas for larger and/or complexly shaped tumours with inner sensitive tissue, such as the prostate, a larger number of fibres is needed to get an acceptable treatment result.

Another aspect that needs to be mentioned is the fact that the computer capacity available is crucial for the time requirements of the optimization algorithm. The computers are rapidly getting faster which is favourable for the optimization. Larger geometries and higher resolutions can thus be considered in the optimization.

Also important to discuss is if the placement of the fibres will work in practice. The point of having a good optimization algorithm is doubtful if the precision of the fibre placement then will turn out to be very bad. Luckily the results from placements of the needles for brachytherapy in the prostate indicate that at least a precision of 1-2 mm should be within reach [14].

Another very important issue is whether our assumptions are reasonable or not. Is the diffusion approximation good enough? Is $\mu_s' >> \mu_a$ for tumour tissue during a treatment? Does the use of many fibres at the same time disturb the fluence rate field in a considerable way? To answer these questions further simulations have to be performed and results from clinical tests must be evaluated.

9 Future Work

In our algorithms we have assumed that each fibre delivers the same light power. One way of improving the algorithm is to allow the fibres to deliver different power, which is equivalent to varying how long time each fibre delivers light during the treatment. If both the fibre's output power and fibre position is to be optimized at once, the optimization problem gets even more complicated compared to only optimizing the positions. For every power you can vary you get one more degree of freedom, so instead of having 18 different parameters (one for each coordinate) you now have 24 parameters (18 coordinates and 6 powers) to optimize.

An easier way is to divide the problem into two parts; one that optimizes the positions using the given fixed powers and one that optimizes the powers using fixed coordinates. By constantly switching between the two optimization algorithms you could probably iteratively find the best powers and positions for the tumour in question.

In our algorithm we have assumed optical homogeneity, using tabulated values of the optical properties. Since the optical properties differ a lot from patient to patient and also within one tissue type, optical homogeneity is a rough approximation [27]. If you somehow possess deeper knowledge about the optical properties of the tumour to be treated and its surrounding tissues you probably want the variations in optical properties to be included in the optimization process. Only by doing this is it possible to get an accurate fluence rate distribution within the tumour.

The weight factor, w_i, used in our algorithm can be seen as a simplification of having a variable absorption coefficient. It will give accurate information about the actual absorbed dose in every voxel if you assume the fluence rate in the voxel to be accurate. Unfortunately the fluence rate is not accurate since variations in the absorption coefficient between voxels will effect the fluence rate distribution in the whole tumour and thus also affect the absorbed dose in each voxel.

One more thing to investigate is how much the needles used for insertion of fibres effect the fluence rate distribution during treatment. If the needles happen to have a too high influence on the fluence rate distribution the disturbance can not be neglected and must be considered in the optimization. One simple way of dealing with the problem is to not allow fibres to be placed too close to each other, which will reduce the influence.

We implemented a fairly simple objective function that seems to perform well, but, there are a lot of other possible objective functions and the one we have chosen might not be the one that performs the best. A thorough search for and a methodical evaluation of promising objective functions ought to be made. Objective functions performing well when applied to closely related cancer treatments such as brachytherapy and cryotherapy might not necessarily be the best for IPDT, as discussed in section 8.6.

Before the optimization program can be used it must be fully integrated with the rest of the software controlling the IPDT-system. The integration with the image delivering apparatus (ultrasound or MRI) must also be done, once a decision is made about which technique to use.

10 Acknowledgements

Most of all we would like to thank our supervisor Ann Johansson who has guided us through this work and helped us with everything, from the first literature searches to the final proofreading of the report. We also want to thank Professor Stefan Andersson-Engels for his guidance.

Further we would like to thank the entire Medical group at the Atomic Physics Department, and especially Florian Forster for learning us more about Matlab.

We also want to thank Johan Axelsson, Alexandra Löwgren, Johan Stensson and Birgitta Strömdahl, our fellow diploma workers and colleagues, for the good company at the office.

Finally we want to thank ourselves and CSN for financially supporting our work.

11 References

1 Berg, R. Laser-based cancer diagnostics and therapy - Tissue optics considerations. 1995. Lund, Sweden, Lund Institute of Technology.
Ref Type: Thesis/Dissertation

2 af Klinteberg, C. On the use of light for the characterization and treatment of malignant tumours. LRAP-245. 1999. Lund, Sweden, Lund Institute of Technology. 1999.
Ref Type: Thesis/Dissertation

3 Wang, I. Photodynamic therapy and laser-based diagnostic studies of malignant tumours. 1999. Lund, Sweden, Lund University.
Ref Type: Thesis/Dissertation

4 Enejder, A. M. K. Light scattering and absorption in tissue - models and measurements. 1997. Lund, Sweden, Lund Institute of Technology.
Ref Type: Thesis/Dissertation

5 Pålsson, S. Methods, instrumentation and mechanisms for optical characterization of tissue and treatment of malignant tumours. 2003.
Ref Type: Thesis/Dissertation

6 C. S. Loh, A. J. MacRobert, J. Bedwell, J. Regula, N. Krasner, and S. G. Bown, Oral versus intravenous administration of 5-aminolevulinic acid for photodynamic therapy, *Br. J. Cancer*, *68* (1993) 41-51.

7 I. A. Boere, D. J. Robinson, H. S. de Bruijn, J. van den Boogert, H. W. Tilanus, H. J. C. M. Sterenborg, and R. W. F. de Bruin, Monitoring in situ dosimetry and protoporphyrin IX fluorescence photobleaching in the normal rat esophagus during 5-aminolevulinic acid photodynamic therapy, *Photochem. Photobiol.*, *78* (2003) 271-2.

8 Eker, C. Optical characterization of tissue for medical diagnostics. LRAP-249. 1999. Lund, Sweden, Lund Institute of Technology. 1999.
Ref Type: Thesis/Dissertation

9 L. O. Svaasand, P. Wyss, M. T. Wyss, Y. Tadir, B. J. Tromberg, and M. W. Berns, Dosimetry model for photodynamic therapy with topically administered photosensitizers, *Lasers Surg. Med.*, *18* (1996) 139-149.

10 J.-L. Boulnois, Photophysical processes in laser-tissue interactions, in R. Ginsburg (ed.), *Laser applications in cardiovascular diseases,* Futura Publishing Company, New York, 1987, pp. 47-66.

11 M. S. Patterson, B. Chance, and B. C. Wilson, Time resolved reflectance and transmittance for the non-invasive measurement of optical properties, *Appl. Opt.*, *28* (1989) 2331-2336.

12 Soto Thompson, M., Johansson, A., Johansson, T., Andersson-Engels, S., Bendsoe, N., Svanberg, K., and Svanberg, S. Clinical system for interstitial photodynamic therapy with combined on-line dosimetry measurements. 2004.
Ref Type: Unpublished Work

13 S. Andersson-Engels, N. Bendsoe, A. Johansson, T. Johansson, S. Pålsson, M. Soto Thompson, K. Svanberg, and S. Svanberg, Integrated system for interstitial photodynamic therapy, Proc. SPIE, Bellingham, WA, 2003, pp. 42-48.

14 L. K. Lee, C. Whitehurst, M. L. Pantelides, and J. V. Moore, An interstitial light assembly for photodynamic therapy in prostatic carcinoma, *Bju International*, *84* (1999) 821-826.

15 M. Soumya and T. H. Foster, Carbogen breathing significantly enhances the penetration of red light in murine tumours *in vivo*, *Phys. Med. Biol.*, *49* (2004) 1891-1904.

16 A. M. K. Nilsson, R. Berg, and S. Andersson-Engels, Measurements of the optical properties of tissue in conjunction with photodynamic therapy, *Appl. Opt.*, *34* (1995) 4609-4619.

17 P. Juzenas, V. Iani, S. Bagdonas, R. Rotomskis, and J. Moan, Fluorescence spectroscopy of normal mouse skin exposed to 5-aminolaevulinic acid and red light, *Journal of Photochemistry and Photobiology B-Biology*, *61* (2001) 78-86.

18 Tabulated Molar Extinction Coefficient for Hemoglobin in Water. Oregon Medical Laser Center . 2003. http://omlc.ogi.edu/spectra/hemoglobin/summary.html
Ref Type: Electronic Citation

19 A. Curnow, J. C. Haller, and S. G. Bown, Oxygen monitoring during 5-aminolaevulinic acid induced photodynamic therapy in normal rat colon. Comparison of continuos and fractionated light regimes., *J. Photochem. Photobiol. B.*, *58* (2000) 149-155.

20 The education center for prostate cancer patients. 2004.
http://www.ecpcp.org/options/5.php
Ref Type: Electronic Citation

21 R. Baissalov, G. A. Sandison, D. Reynolds, and K. Muldrew, Simultaneous optimization of cryoprobe placement and thermal protocol for cryosurgery, *Phys. Med. Biol.*, *46* (2001) 1799-1814.

22 M. Lahanas, D. Baltas, and N. Zamboglou, A hybrid evolutionary algorithm for multi-objective anatomy-based dose optimization in high-dose-rate brachytherapy, *Phys. Med. Biol.*, *48* (2003) 399-415.

23 S. Yoo, M. E. Kowalok, B. R. Thomadsen, and D. L. Henderson, Treatment planning for prostate brachytherapy using region of interest adjoint functions and a greedy heuristic, *Phys. Med. Biol.*, *48* (2003) 4077-4090.

24 M. Goldberg and M. Unger, Lung cancer. Diagnostic tools, *Chest Surg. Clin. N. Am.*, *10* (2000) 763-79, vii.

25 Ohlsson, N. and Rylow, O. Development of a multifibre system for interstitial photodynamic therapy of malignant tumours. LRAP-240. 1998. Lund, Sweden, Lund Institute of Technology. Lund Reports on Atomic Physics.
Ref Type: Thesis/Dissertation

26 D. E. Goldberg, A gentle introduction to genetic algorithms, *Genetic algorithms in search, optimization, and machine learning,* Addison-Wesley publishing company, Inc, 2004, pp. 1-25.

27 S. L. Jacques, Variability of tissue optical properties in cancer patients receiving photodynamic therapy, Preceedings of the second joint EMBS/BMES conference, 2002, pp. 2283-2284.

12 Appendix: Tumour geometries

Tumour 1 - arbitrarily shaped, 547 voxels

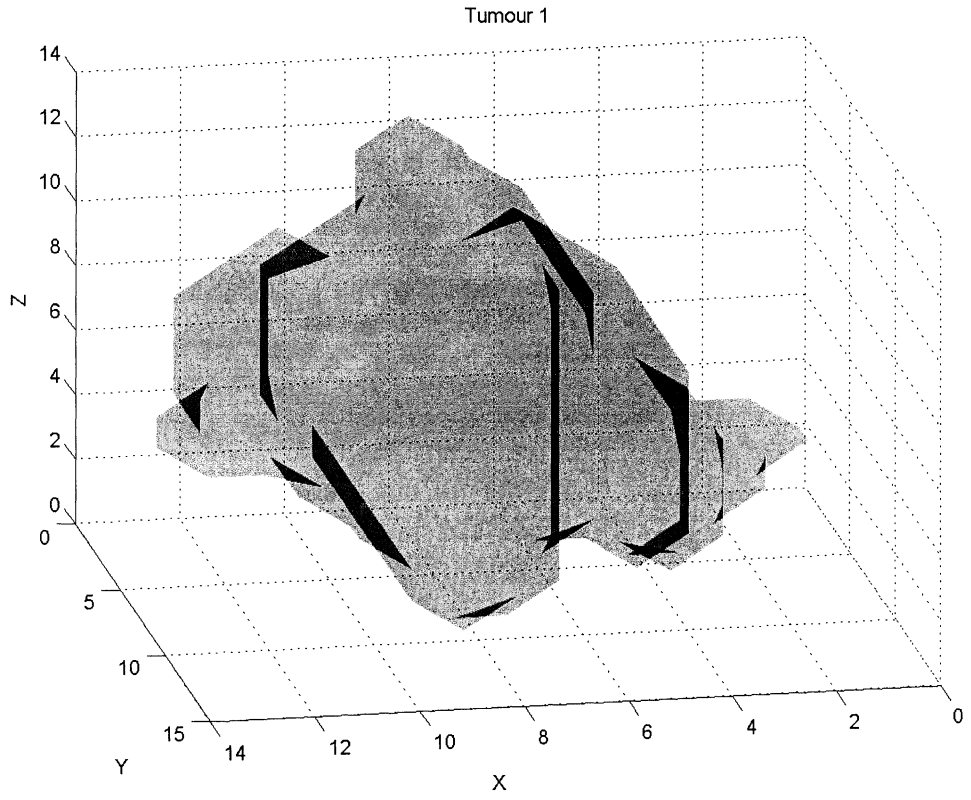

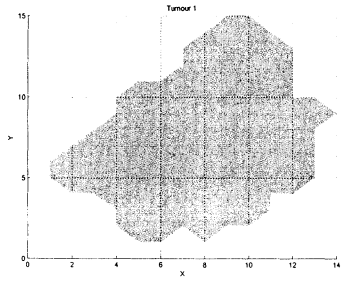

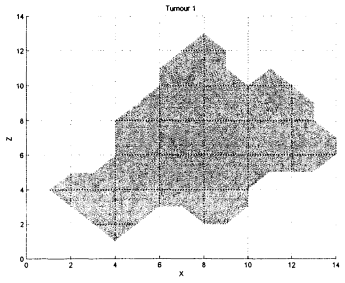

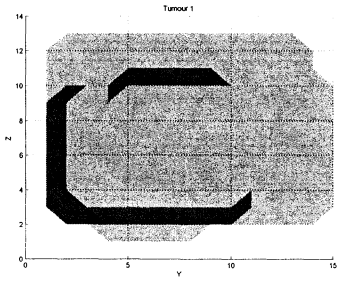

Tumour 2 – arbitrarily shaped, 5371 voxels

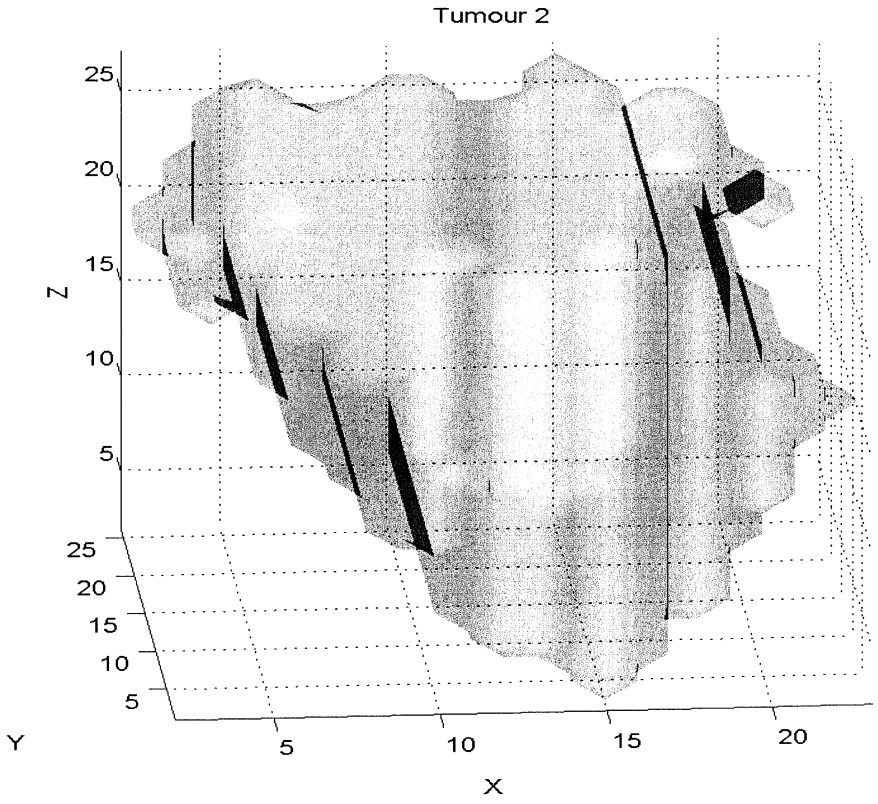

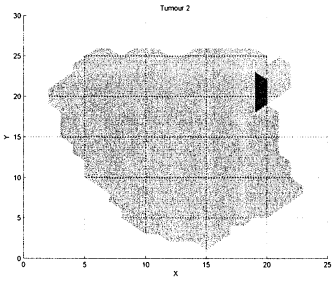

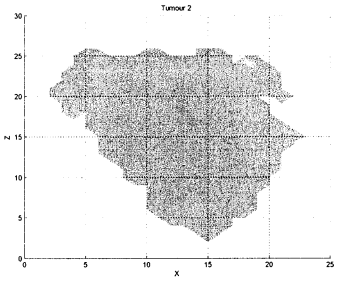

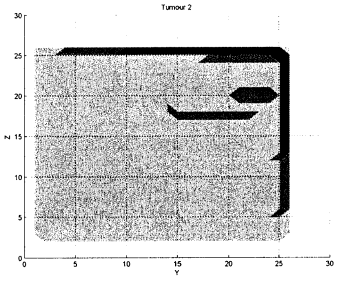

Prostate geometry, 1874 voxels